

# Eruptive history and $^{40}\text{Ar}/^{39}\text{Ar}$ geochronology of the Milos volcanic field, Greece

Xiaolong Zhou<sup>1</sup>, Klaudia Kuiper<sup>1</sup>, Jan Wijbrans<sup>1</sup>, Katharina Boehm<sup>1</sup>, Pieter Vroon<sup>1</sup>

<sup>1</sup>Department of Earth Sciences, VU University Amsterdam, De Boelelaan 1085, 1081 HV Amsterdam, The Netherlands.

Correspondence to: Xiaolong Zhou (z.x.l.zhou@vu.nl)

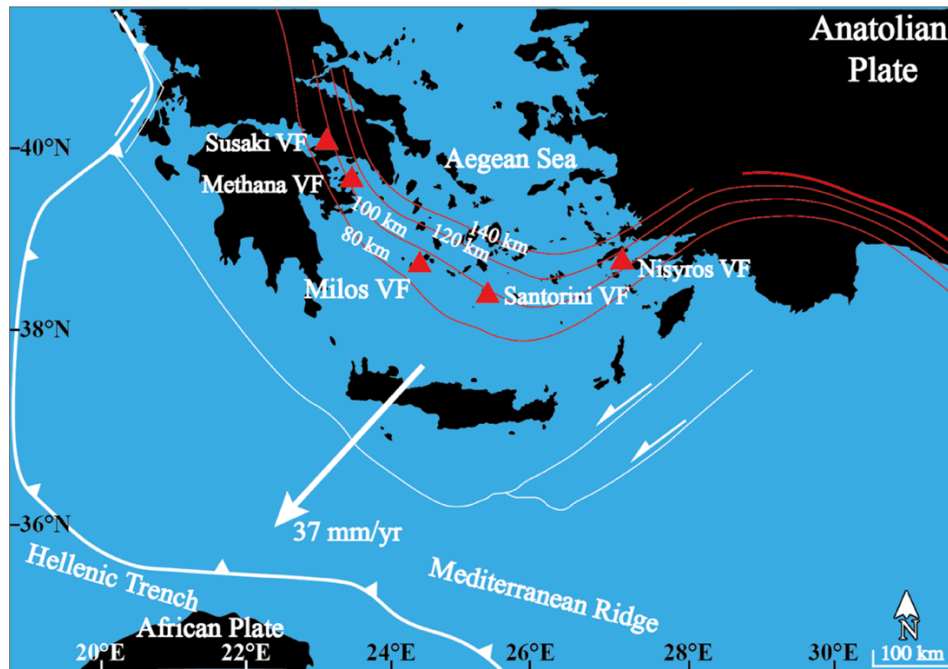
**Abstract.** High-resolution geochronology is essential for determining the growth-rate of volcanoes, which is one of the key factors for establishing the periodicity of volcanic eruptions. However, there are less high-resolution eruptive histories ( $>10^6$  years) determined for long-lived submarine arc volcanic complexes than for subaerial complexes, since submarine volcanoes are far more difficult to observe than subaerial ones. In this study, high-resolution geochronology and major element data are presented for Milos Volcanic Field (VF) in the South Aegean Volcanic Arc, Greece. The Milos VF has been active for over 3 Ma, and the first two million years of its eruptive history occurred in a submarine setting that has been emerged above sea level. The long submarine volcanic history of the Milos VF makes it an excellent natural laboratory to study the growth-rate of a long-lived submarine arc volcanic complex. This study reports twenty-one new high-precision  $^{40}\text{Ar}/^{39}\text{Ar}$  ages and major element compositions for eleven volcanic units of the Milos VF. This allows us to divide the Milos volcanic history into at least three periods of different long-term volumetric volcanic output rate ( $Q_e$ ). Period I (submarine,  $\sim 3.3$ -2.13 Ma) and III (subaerial, 1.48 Ma-present) have low  $Q_e$  of  $0.9 \pm 0.5 \times 10^{-5} \text{ km}^3 \cdot \text{yr}^{-1}$  and  $0.25 \pm 0.05 \times 10^{-5} \text{ km}^3 \cdot \text{yr}^{-1}$ , respectively. Period II (submarine, 2.13 - 1.48 Ma) has a 3-12 times higher  $Q_e$  of  $3.0 \pm 1.7 \times 10^{-5} \text{ km}^3 \cdot \text{yr}^{-1}$ . The  $Q_e$  of the Milos VF is 2-3 orders of magnitude lower than the average for rhyolitic systems and continental arcs.

## 1 Introduction

Short-term eruptive histories and compositional variations of lavas and pyroclastic deposits of many arc volcanic fields are well established. However, high-resolution eruptive histories that extend back  $> 10^5$ - $10^6$  years have been determined only for a handful of long-lived subaerial arc volcanic complexes. Some examples are: Mount Adams (Hildreth and Lanphere, 1994), Tatará–San Pedro (Singer et al., 1997), Santorini (Druitt et al., 1999), Montserrat (Cole et al., 2002), Mount Baker (Hildreth et al., 2003a), Katmai (Hildreth et al., 2003b), and Ceboruco–San Pedro (Frey et al., 2004). To establish the growth-rate of volcanic complexes and disentangle the processes responsible for the eruption, fractionation, storage, and transport of magmas over time, comprehensive geological studies are required. These include detailed field mapping, sampling, high-resolution geochronology and geochemical analysis. Based on these integrated studies, the growth-rate of volcanoes can be determined to establish the periodicity of effusive and explosive volcanism.

The Milos Volcanic Field (VF) is a long-lived volcanic complex that has been active for over 3 Ma. The Milos VF erupted for a significant part of its life below sea level, similar to the other well studied volcanic structures in the eastern Mediterranean (Fytikas et al., 1986; Stewart and McPhie, 2006). The eruptive history of the Milos VF has been examined with a broad range of chronostratigraphic techniques such as K-Ar, U-Pb, fission track,  $^{14}\text{C}$  and biostratigraphy (e.g. Angelier et al., 1977, Fytikas et al., 1976, 1986, Traineau and Dalabakis, 1989, Matsuda et al., 1999, Stewart and McPhie, 2006, Van Hinsbergen et al., 2004 and Calvo et al., 2012). However, most of the published ages have been measured using the less precise K-Ar or fission track methods, and modern, high precision  $^{40}\text{Ar}/^{39}\text{Ar}$  ages for the Milos VF have not been published so far. In this study, (1) we provide high-precision  $^{40}\text{Ar}/^{39}\text{Ar}$  geochronology of key volcanic units of the Milos VF and (2) refine the stratigraphic

38 framework of the Milos VF with the new high-precision  $^{40}\text{Ar}/^{39}\text{Ar}$  ages and major element composition. (3) We also quantify  
39 and constrain the compositional and volumetric temporal evolution of volcanic products of the Milos VF.



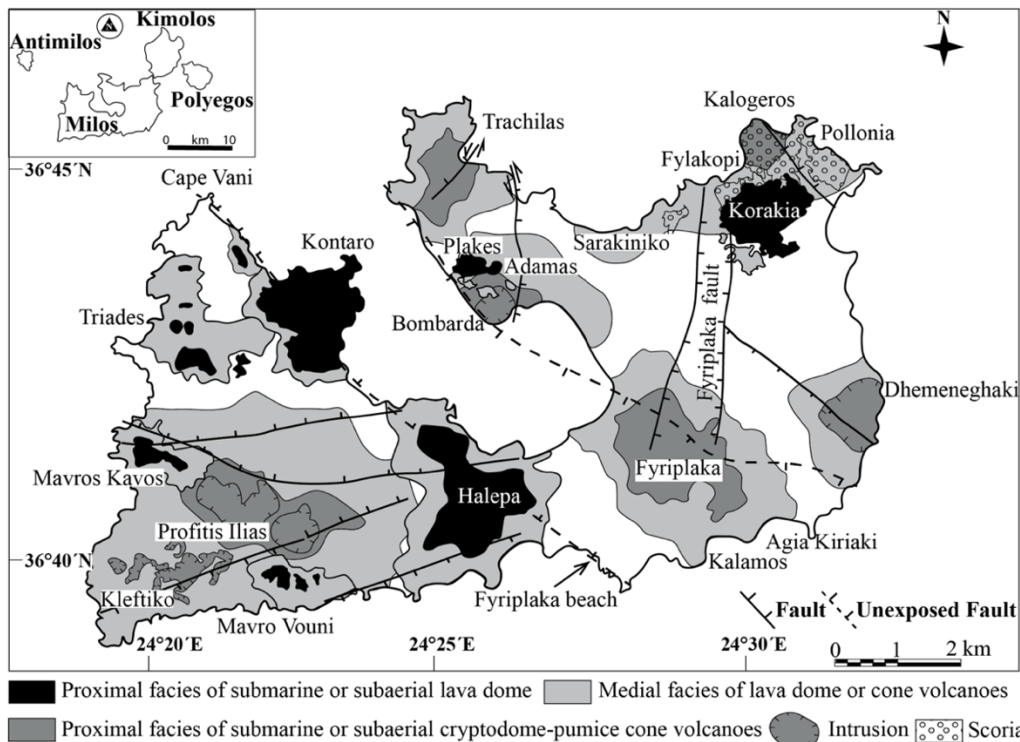
40  
41 **Figure 1. Map of the South Aegean Volcanic Arc (SAVA). Red triangles indicate Volcanic Fields (VF): Susaki, Methana and Milos**  
42 **VFs in the western SAVA, Santorini VF in the centre and Nisyros VF in the eastern SAVA. Red contour lines show the depth to**  
43 **the Benioff zone (Hayes et al., 2018). The white arrow represents the GPS-determined plate velocity of the Aegean microplate**  
44 **relative to the African plate from Doglioni et al. (2002).**

### 45 1.1 Geological setting

46 The Milos VF is part of the South Aegean Volcanic Arc (SAVA), an arc which was formed in the eastern Mediterranean by  
47 subduction of the African plate beneath the Aegean microplate (Figure 1, Nicholls, 1971; Spakman et al., 1988; Duermeijer et  
48 al., 2000; Pe-Piper and Piper, 2007; Rontogianni et al., 2011). The present-day Benioff zone is located approximately 90 km  
49 underneath Milos (Hayes et al., 2018). The upper plate is influenced by extensional tectonics (e.g. McKenzie, 1978; Pe-Piper  
50 and Piper, 2013), which is evident on the island of Milos as horst and graben structures (Figure 2).

51 The Milos VF is exposed on the islands of the Milos archipelago: Milos, Antimilos, Kimolos and Polyegos. The focus of this  
52 study is Milos which has a surface area of 151 km<sup>2</sup>. The geology and volcanology of Milos have been extensively studied in  
53 the last 100 years. The first geological map was produced by Sonder (1924). This work was extended by Fytikas et al. (1976)  
54 and Angelier et al. (1977) and the subsequent publications of Fytikas et al. (1986) and Fytikas (1989). Interpretations based on  
55 volcanic facies of the complete stratigraphy were made by Stewart and McPhie (2003, 2006). More detailed studies of single  
56 volcanic centres (e.g. Bombarda volcano and Fyriplaka complex) were published by Campos Venuti and Rossi (1996) and  
57 Rinaldi et al. (2003). Milos has also been extensively studied for its epithermal gold mineralization, summarized by Alfieris  
58 et al. (2013). Milos was known during the Neolithic period for its export of high-quality obsidian. Today the main export  
59 product is kaolinite mined from hydrothermally altered felsic volcanic units in the centre of the island (e.g. Alfieris et al.,  
60 2013).

61 The geology of Milos can be divided into four main units: (1) metamorphic basement, (2) Neogene sedimentary rocks, (3)  
62 volcanic sequences and (4) the alluvial cover. The metamorphic basement crops out at the southwest, south and southeast of  
63 Milos (Figure 3) and is also found as clasts in many volcanic units. The metamorphic rocks include lawsonite-free jadeite  
64 eclogite, lawsonite eclogite, glaucophane schist, quartz-muscovite-chlorite and chlorite-amphibole schist (Fytikas et al., 1976,  
65 1986; Grasemann et al., 2018; Kornprobst et al., 1979). The exposed units belong to the Cycladic Blueschist Unit (Lower  
66 Cycladic nappe), whereas eclogite pebbles in the phreatic eruption products called “green lahar” by Fytikas (1977) are derived  
67 from the Upper Cycladic Nappe (Grasemann et al., 2018).



68  
69  
70  
71

**Figure 2. Distribution of the proximal and medial facies of the submarine pumice cone/cryptodome volcanoes, submarine, submarine-subaerial and subaerial domes and rhyolitic complexes (tuff cone and associated lava) of Milos, modified after Fytikas et al. (1986) and Stewart and McPhie (2006). The distal facies of Stewart and McPhie (2006) is not shown.**

72  
73  
74  
75  
76  
77  
78  
79  
80  
81  
82

On top of this metamorphic basement, Neogene fossiliferous marine sedimentary rocks were deposited (e.g. Van Hinsbergen et al. 2004). This sedimentary sequence can be divided into a lower unit A and upper unit B that is unconformably overlain by volcanoclastic sediments (Van Hinsbergen et al., 2004). Unit A is 80 m thick and consists of fluvatile-lacustrine, brackish and shallow marine conglomerate, sandstone, dolomite and limestone. Unit B is 25-60 m thick and consists of sandstone overlain by a succession of alternating marls and sapropels, suggesting a deeper marine setting (Van Hinsbergen et al., 2004). Five volcanic ash layers that contain biotite are found in this Neogene sedimentary sequence, either suggesting that volcanic eruptions in small volume already occurred in the Milos area or that these ash layers are derived from larger eruptions of volcanic centres further away from Milos (van Hinsbergen et al., 2004). Age determinations by bio-magneto- and cyclostratigraphy suggested that deposition of Unit A started at approximately 5 Ma, and that Milos subsided 900 m in 0.6 Ma (Van Hinsbergen et al. 2004) due to extension. This subsidence happened ca 1.0-1.5 Ma before the onset of the main phase of Pliocene- recent volcanism on Milos.

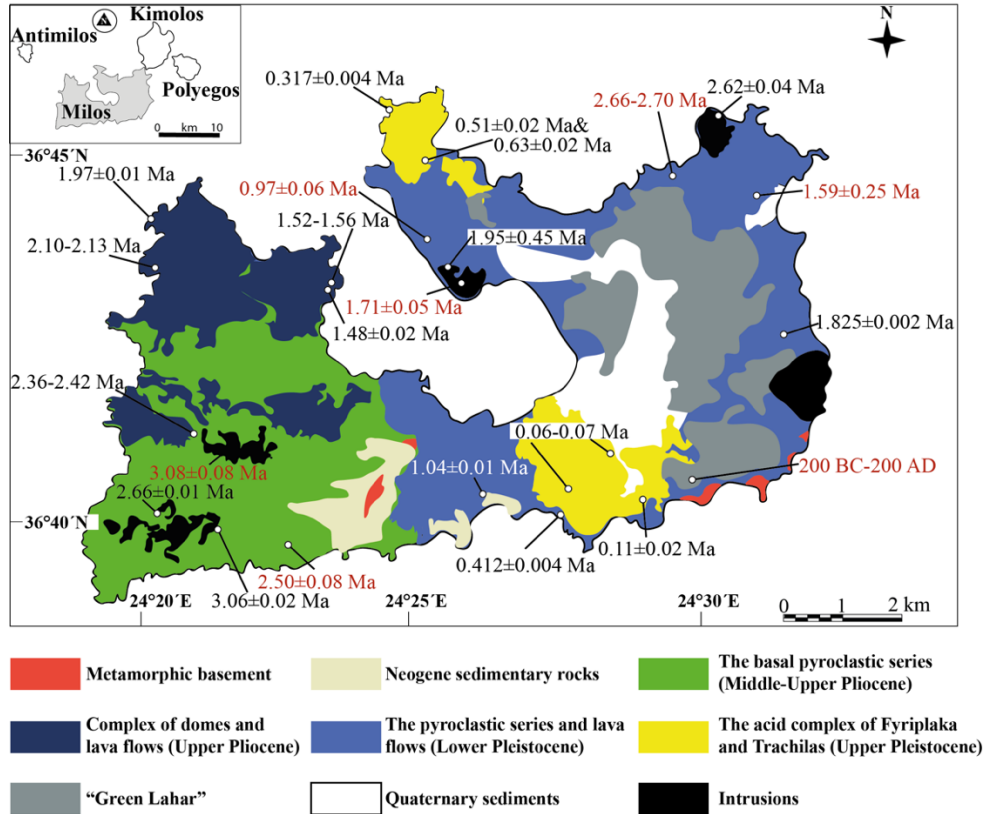
83  
84  
85  
86  
87  
88  
89  
90  
91

The Pliocene-recent volcanic sequence of Milos has been subdivided into different units by Angelier et al. (1977) and Fytikas et al. (1986). In addition, Stewart and McPhie (2006) provided a detailed facies analysis of the different volcanic units. The subdivision by Angelier et al. (1977) is not constrained well due to their limited amount of age data. The subdivision of volcanic units by Fytikas et al. (1986) and facies descriptions of Stewart and McPhie (2006) are summarized below. It is important to note that according to Stewart and McPhie (2006), the five volcanic cycles described by Fytikas et al. (1986) are difficult to match with existing age data and the continuous progression in volcanic construction (Fig. 4). For example, the first phase of Fytikas et al. (1986), the Basal Pyroclastic Series, contains the large pumice cone-cryptodome volcanoes according to Stewart and McPhie (2006). Two of these pumice-cone cryptodome volcanoes are much younger and intercalated between the Complex of Domes and Lava Flows (CDLF) of Fytikas et al. (1986).

92  
93  
94  
95

The first volcanic unit deposited in the Milos area is the Basal Pyroclastic Series (BPS) (Fytikas et al., 1986) or submarine felsic cryptodome-pumice cone volcanoes (Stewart and McPhie, 2006, Figure 2-4). This unit consists of thickly bedded pumice breccia with a rhyolitic-dacitic composition. These rhyolites-dacites are aphyric or contain quartz-feldspar±biotite phenocrysts. Graded sandstone and bioturbated and fossil rich (in-situ bivalve shells) mudstone are intercalated, indicating a marine

96 environment and a water depth of several hundreds of meters (e.g. Stewart, 2003; Stewart and McPhie, 2006), whereas later  
 97 degassed magmas with a similar composition intruded as sills and cryptodomes. The BPS has been strongly affected by  
 98 hydrothermal fluids, especially the proximal deposits (e.g. Kilias et al., 2001).



99  
 100 **Figure 3. Simplified geological map of Milos with our <sup>40</sup>Ar/<sup>39</sup>Ar ages and sample locations of key volcanic deposits, modified after**  
 101 **Stewart and McPhie (2006) and Grasmann et al. (2018). The stratigraphic units of Milos are from Fytikas et al. (1986). Age data**  
 102 **from this study are in black, published ages are shown in red (Angelier et al., 1977, Fytikas et al., 1986, Traineau and Dalabakis,**  
 103 **1989, and Stewart and McPhie, 2006). The "Green Lahar" (Fytikas, 1977) consists of deposits from multiple phreatic explosions**  
 104 **and contains fragments of metamorphic, sedimentary and volcanic rocks.**

105 The second volcanic unit was named the Complex of Domes and Lava Flows (CDLF, Fytikas et al., 1986) and the volcanic  
 106 facies of this unit are described as the submarine dacitic and andesitic domes by Stewart and McPhie (2006). This phase of  
 107 effusive submarine volcanism was predominantly andesitic/dacitic in composition and produced microcrystalline rocks with  
 108 phenocrysts of pyroxene, amphibole, biotite and plagioclase. The eruption centres were mainly located along NNE faults and  
 109 formed up to 300 m thick deposits extending over areas of 2.5 to 10 km<sup>2</sup> around the eruption centres. In the north-eastern part  
 110 of Milos, an andesitic scoria cone provided scoria lapilli and bombs to deeper water settings. Sandstone intercalated in the  
 111 CDLF contains both igneous and metamorphic minerals suggesting input from the basement. Rounded pebbles of rhyolite and  
 112 dacite indicate that some of the volcanic deposits were above sea level, or in very shallow, near shore environments (e.g.  
 113 Stewart and McPhie, 2006).

114 The third volcanic unit is called the Pyroclastic Series and Lava Domes (PSLD) by Fytikas et al. (1986) and belongs to  
 115 submarine-to-subaerial dacitic and andesitic lava domes of Stewart and McPhie (2006). This highly variable group is  
 116 dominated by rhyolitic, dacitic and andesitic lavas, domes, pyroclastic deposits and felsic pumiceous sediments (Stewart and  
 117 McPhie, 2006). Thickness varies between 50-200 m, and the deposits are located in the eastern and northern parts of Milos  
 118 (Figure 2 and 3). The initial pyroclastic layers were subaqueously deposited and the extrusion of a dome resulted in the  
 119 deposition of talus around the margins by mass flow. On top of the dome sand- and siltstone with fossils (Ostrea fossil  
 120 assemblage) and traction-current structures suggest that the top of the dome was above wave base. The youngest deposits of  
 121 this unit are dacitic and andesitic lavas and domes. These domes generated subaerial block-and-ash flow and surge deposits.  
 122 Paleosols within these deposits are a clear indicator that some areas were above sea level. The last unit of the PSLD is

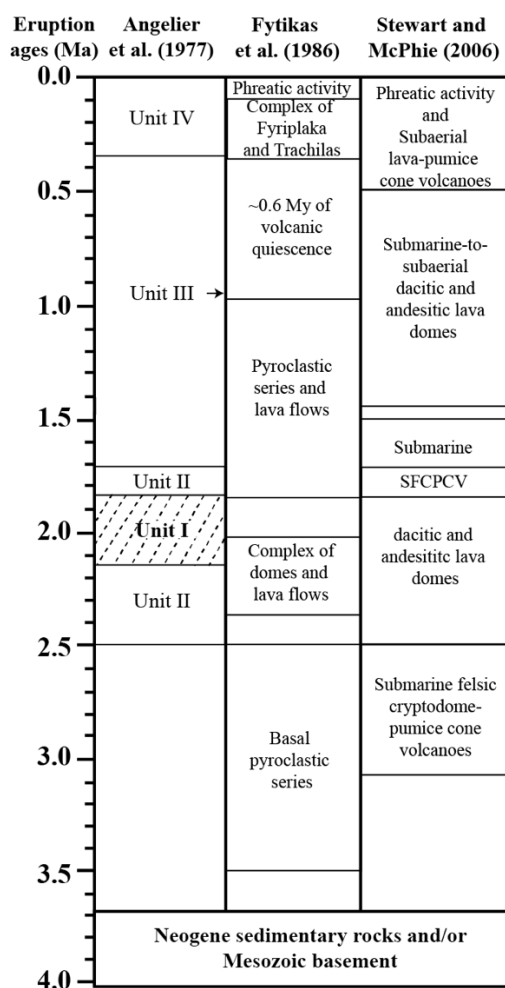
123 represented by large subaerial rhyolitic lava that contains quartz and biotite phenocrysts and is found near Halepa in the south-  
 124 central part of Milos.

125 **Table 1. Published eruption ages of stratigraphic units of the island of Milos**

Stratigraphy	Sample	Mineral	Location	Petrology	K <sub>2</sub> O (wt.%)	Age (Ma)	± 1σ	Reference
Unit IV	Angelier_1	Unknown	Fyriplaka	Rhyolite	-	-	-	
Unit III	Angelier_2	Unknown	Halepa	Rhyolite	2.44	0.95	0.06	
Unit II	Angelier_3	Unknown	Triades	Dacite	1.47	1.71	0.08	Angelier et al. (1977)
	Angelier_4	Unknown	Kleftico	Andesite	1.77	2.33	0.09	
	Angelier_5	Unknown	Kleftico	Andesite	1.45	2.50	0.09	
Unit I	Angelier_6	Unknown	Adamas	Rhyolite	2.90	2.15	0.08	
	Angelier_7	Unknown	Dhemenehaki	Rhyolite	2.75	1.84	0.08	
Phreatic activity	Gif-7358&7359	Carbonized wood	Agia Kiriaki	Lahar deposits	-	200 BC-200 AD		Trainau and Dalabakis (1989)
CFT	M196	Unknown	Fyriplaka	Rhyolite	2.9	0.09	0.02	Fytikas et al. (1976, 1986)
	M194	Unknown	Fyriplaka	Rhyolite	2.85	0.14	0.03	
	M168	Unknown	Trachilas	Rhyolite	3.91	0.37	0.09	
	M-48	Biotite	NW of Filiplaka	Rhyolite	6.41	0.48	0.05	
PSLD	M-OB1	Groundmass	N of Dhemenehaki	Obsidian	2.53	0.88	0.18	Fytikas et al. (1976, 1986)
	M27	Unknown	Plakes	Dacite	1.87	0.97	0.06	
	M-OB2	Groundmass	Bombarda	Obsidian	2.73	1.47	0.05	
	M103	Unknown	near Pollonia	Andesite	1.87	1.59	0.25	
	M146	Unknown	1km NW of Adamas	Rhyolite	3.09	1.71	0.05	
	M110	Unknown	Sarakiniko	Dacite	2.57	1.85	0.10	Matsuda et al. (1999)
	MI-1	Lava	Plakes	Dacite	2.07	0.80	0.10	
	MI-4	Lava	Plakes	Dacite	2.32	1.20	0.10	
	MIL130	Zircon	Triades	Dacite	-	1.44	0.08	Stewart and McPhie (2006)
	Fission track1	Groundmass	Adamas	Obsidian	-	1.54	0.18	Bigazzi and Radi (1981)
Fission track2	Groundmass	Bombarda	Obsidian	-	1.57	0.15		
Fission track3	Groundmass	Bombarda-Adamas	Obsidian	-	1.57	0.12	Arias et al. (2006)	
Fission track3	Groundmass	Dhemenehaki	Obsidian	-	1.60	0.06		
CDLF	M1	Unknown	Aghios, near Triades	Rhyolite	3.32	2.04	0.09	Fytikas et al. (1976, 1986)
	M66	Unknown	~1 km NW of Adamas	Dacite	2.61	2.03	0.06	
	M156	Unknown	Angathia, near Triades	Dacite	2.84	2.38	0.10	
	MIL243	Zircon	Triades	Dacite	-	2.18	0.09	Stewart and McPhie (2006)
BPS	MIL365	Zircon	Filakopi	Rhyolite	-	2.66	0.07	Stewart and McPhie (2006)
	MIL343	Zircon	Kalogeros cryptodome	Dacite	-	2.70	0.04	
	M164	Unknown	Kleftico	Rhyolite	2.84	3.08	0.08	Fytikas et al. (1976, 1986)
	M163	Unknown	Kleftico	Andesite	1.18	3.50	0.14	

126 Angelier et al. (1977) do not provide sample names, only numbers for the sample locations. Here the location is given after “Angelier\_”  
 127 (Angelier et al. 1977, their Fig. 3). Abbreviations: BPS=Basal pyroclastic series; CDLF=Complex of domes and lava flows;  
 128 PSLD=Pyroclastic series and lava domes; CTF=Complexes of Trachilas and Fyriplaka. See more details in Figure. 4.

129 The fourth unit consists of the subaerially constructed rhyolitic Complexes of Trachilas and Fyriplaka (CTF) (Fytikas et al.,  
 130 1986), which Stewart and McPhie (2006) interpreted as subaerial rhyolitic lava-pumice cones. These two volcanic complexes  
 131 are built from rhyolitic pumice deposits and lavas that contain quartz and biotite phenocrysts (10-20 modal %). The deposits  
 132 have a maximum thickness of 120 m and decrease to several meters thickness in the distal parts. Basement-derived schist is  
 133 found as lithic clasts (Fytikas et al., 1986). In addition, the Kalamos rhyolitic lava dome, which outcrops on the southern coast  
 134 of Milos, produced lava that spread westwards to the Fyriplaka beach (Figure 2). This lava belongs to this fourth phase and is  
 135 probably derived from an older volcano and not the Fyriplaka complex (Campos Venuti and Rossi, 1996).  
 136 The fifth volcanic unit comprises deposits from phreatic activity, especially in the northern part of the Zefiria Graben and near  
 137 Agia Kiriaki (Figure 2 of Stewart and McPhie, 2006). Many overlapping craters are surrounded by lithic breccias that are  
 138 composed of variably altered metamorphic basement clasts and volcanic clasts. This phreatic activity has continued into  
 139 historic times (Trainau and Dalabakis, 1989). Fytikas et al. (1986) referred to this unit as “green lahar”, although it indicated  
 140 that this deposit is not a lahar but the product of phreatic eruptions in the last 0.2 Ma.



141  
 142 **Figure 4. Previous proposed stratigraphic frameworks for Milos by Angelier et al. (1977), Fytikas et al. (1986) and Stewart and**  
 143 **McPhie (2006). Volcanic unit II of Angelier et al. (1977) contains unit I. Stewart and McPhie (2006) described the volcanic faces of**  
 144 **Milos mainly based on the geochronological works of Angelier et al. (1977) and Fytikas et al. (1986). Abbreviation:**  
 145 **SFCPCV=Submarine felsic cryptodome-pumice cone volcanoes.**

146 **1.2 Previous geochronological studies**

147 Previous geochronological work is summarised in Table 1. Angelier et al. (1977) reported six K-Ar ages (0.95-2.50 Ma). These  
 148 ages were used in combination with field observations to divide the Milos volcanic succession into four units. However, the  
 149 samples from Fyriplaka, the fourth unit, were too young to be dated by Angelier et al. (1977). Fytikas et al. (1976, 1986)  
 150 published 16 K-Ar ages for Milos (0.09-3.50 Ma) including an age of 0.09-0.14 Ma for the Fyriplaka complex. Fytikas et al.  
 151 (1986) also obtained 3 K-Ar ages for Antimilos ( $0.32 \pm 0.05$  Ma), Kimolos ( $3.34 \pm 0.06$  Ma) and Polyegos ( $2.34 \pm 0.17$  Ma).

152 Trainau and Dalabakis (1989) dated the very young phreatic deposits by  $^{14}\text{C}$  dating and found ages between 200 BC and 200  
153 AD. Matsuda et al. (1999) published two K-Ar ages of  $0.8 \pm 0.1$  (MI-1) and  $1.2 \pm 0.1$  Ma (MI-4) for the Plakes dome that was  
154 also studied by Fytikas et al. (1986). Bigazzi and Radi (1981) published two fission track ages of  $1.54 \pm 0.18$  and  $1.57 \pm 0.15$   
155 Ma for obsidians of Bombarda-Adamas and Demenaghaki, respectively. Later fission track studies by Arias et al. (2006) ( $1.57$   
156  $\pm 0.12$  and  $1.60 \pm 0.06$  Ma) confirmed these ages. The fission track ages are younger than the K-Ar ages given by Angelier et  
157 al. (1977;  $1.84 \pm 0.08$  Ma for Demenaghaki) and Fytikas et al. (1986;  $1.71 \pm 0.05$  Ma for Bombarda). In the most recent  
158 geochronological study of the Milos VF, Stewart and McPhie (2006) published 4 SHRIMP U/Pb zircon ages: Triades dacite  
159 facies ( $1.44 \pm 0.08$  and  $2.18 \pm 0.09$  Ma), Kalogeros cryptodome ( $2.70 \pm 0.04$  Ma) and the Fylakopi Pumice Breccia ( $2.66 \pm$   
160  $0.07$  Ma). All uncertainties reported here are one standard deviation uncertainties as reported in the original publications,  
161 except for the  $^{14}\text{C}$  ages for which uncertainties were not specified.

162 The previous geochronological work for the MVF is mainly based on K-Ar ages. However, K-Ar ages may show undesirable  
163 and unresolvable scatter due to various problems: (1) inaccurate determination of radiogenic argon due to either incorporation  
164 of excess argon or incomplete degassing of argon during the experiments; (2) inclusion of cumulate or wall rock phenocrysts  
165 in bulk analyses; (3) disturbance of a variety of geological processes such as slow cooling, thermal reheating; (4) unrecognized  
166 heterogeneities due to separate measurements of potassium and argon content by different methods; (5) requirement of  
167 relatively large quantities (milligrams) of pure sample (e.g. Lee, 2015). In addition to these methodological issues, in the case  
168 of Milos we observe that hydrothermal alteration caused substantial kaolinitisation, in particular the felsic volcanic samples,  
169 that most likely has affected the K-Ar systematics. Some of these issues are also valid for the  $^{40}\text{Ar}/^{39}\text{Ar}$  method. However, the  
170 K-Ar method does not allow testing if ages are compromised.

171  $^{40}\text{Ar}/^{39}\text{Ar}$  ages only need isotopes of argon to be measured from a single aliquot of sample with the same equipment that can  
172 eliminate some of the problems with sample inhomogeneity. Furthermore, step heating and multiple single fusion experiments  
173 can shed light on sample inhomogeneity due to partial alteration effects. The high sensitivity of modern noble gas mass  
174 spectrometers for  $^{40}\text{Ar}/^{39}\text{Ar}$  measurements results in very small sample amounts needed for analysis, that can yield more  
175 information on the thermal or alteration histories than larger samples. Moreover, other argon isotopes ( $^{36}\text{Ar}$ ,  $^{37}\text{Ar}$  and  $^{38}\text{Ar}$ ) can  
176 be used to infer some information about the chemical compositions (i.e. Ca and Cl) of samples. A high-resolution laser  
177 incremental heating method of  $^{40}\text{Ar}/^{39}\text{Ar}$  dating allows us to resolve the admixture of phenocryst-hosted inherited  $^{40}\text{Ar}$  in the  
178 final temperature steps of the incremental step heating experiments.

## 179 2 Methods

### 180 2.1 Mineral separation and sample preparation

181 Samples were collected from all major volcanic units on Milos island based on the studies of Fytikas et al. (1986), Stewart and  
182 McPhie (2006) and our own observations in the field. Photos of the sample locations and thin sections can be found in  
183 supplementary material I. Approximately 2 kg of fresh pumice clasts or lava was sampled from each unit. Samples were cut  
184 into  $\sim 5\text{ cm}^3$  cubes using a diamond saw to remove potentially altered surfaces and obtain the fresh interior parts. These cubes  
185 were ultra-sonicated for 30 minutes in demi-water to remove dust and seawater and dried in an oven overnight at  $50\text{ }^\circ\text{C}$ . Dry  
186 sample cubes were crushed in a steel jaw crusher, and this fraction was split into two portions of roughly equal size. One of  
187 them was powdered in an agate shatter box and agate ball mill to a grain size of less than  $2\text{ }\mu\text{m}$  for the major-element analysis.  
188 The second fraction was sieved to obtain a grain size of  $250\text{-}500\text{ }\mu\text{m}$  for  $^{40}\text{Ar}/^{39}\text{Ar}$  dating.

189 Heavy liquids density separation techniques (IJlst, 1973) were used to purify mineral separates (groundmass, biotite, amphibole)  
190 required for the  $^{40}\text{Ar}/^{39}\text{Ar}$  dating. Different densities of heavy liquids were used to obtain groundmass ( $2700 \leq \rho \leq 3000\text{ kg.m}^{-3}$ ),  
191 biotite ( $2900 \leq \rho \leq 3100\text{ kg.m}^{-3}$ ) and/or amphibole ( $\sim 3100 \leq \rho \leq 3200\text{ kg.m}^{-3}$ ). A Franz Isodynamic Magnetic separator was  
192 used to remove the magnetic minerals from the non-magnetic minerals and groundmass. The samples for  $^{40}\text{Ar}/^{39}\text{Ar}$  analysis

193 were purified by handpicking under a binocular optical microscope to select mineral grains without visible alteration and  
194 inclusions.

## 195 2.2 $^{40}\text{Ar}/^{39}\text{Ar}$ dating

196 The mineral and groundmass samples were wrapped in either 6- or 9-mm aluminium foil and packed in 20 mm aluminium  
197 cups, that were vertically stacked. Based on stratigraphy and previous geochronological constraints >1 Ma samples and the <1  
198 Ma samples were irradiated for 7 and 1 hours respectively in irradiation batches VU108 and VU110 in the Cadmium-Lined  
199 in-Core Irradiation Tube (CLICIT) facility of the Oregon State University Training Research, Isotopes, General Atomics  
200 (TRIGA) reactor. The neutron flux for all irradiations was monitored by standard bracketing using the Drachenfels sanidine  
201 (DRA;  $25.52 \pm 0.08$  Ma, modified from Wijbrans et al., 1995 and calibrated relative to Kuiper et al., 2008) and Fish Canyon  
202 Tuff sanidine (FCs;  $28.201 \pm 0.023$  Ma, Kuiper et al., 2008) with Min et al. (2000) decay constants.

203 In total, 24 samples (8 groundmasses, 15 biotites and 2 amphiboles, for sample G15M0026 both biotite and amphibole were  
204 analysed) were measured by either  $^{40}\text{Ar}/^{39}\text{Ar}$  fusion and/or incremental heating techniques. For incremental heating  
205 experiments, 80-100 grains per sample were loaded into a 25-hole (surface per hole  $\sim 36$  mm<sup>2</sup>) copper tray together with single  
206 grain standards in  $\sim 12$  mm<sup>2</sup> holes. The tray was prebaked in vacuum ( $10^{-5}$ - $10^{-6}$  mbar) at 250 °C overnight to remove  
207 atmospheric argon and subsequently baked overnight at 120 °C in the ultra-high vacuum sample chamber ( $<5 \times 10^{-9}$  mbar) and  
208 purification system connected to a Thermo Scientific Helix MC mass spectrometer.

209 Samples and standards were heated with a focused laser beam at 8 % power using a 50W CW CO<sub>2</sub> laser. The released gas was  
210 cleaned by exposure to a cold trap cooled by a Lauda cooler at -70 °C, a SAES NP10 at 400 °C, Ti sponge at 500 °C and cold  
211 SAES ST172 Fe-V-Zr sintered metal. The five isotopes of argon were measured simultaneously on five different collectors:  
212  $^{40}\text{Ar}$  on the H2-Faraday,  $^{39}\text{Ar}$  on the H1-Faraday or the H1-CDD,  $^{38}\text{Ar}$  on the AX-CDD,  $^{37}\text{Ar}$  on the L1-CDD and  $^{36}\text{Ar}$  on the  
213 L2-CDD for 15 cycles with 33 seconds integration time (CDD: compact discrete dynodes). The Faraday cups on H2 and H1  
214 were equipped with  $10^{13}$  Ω amplifiers. Procedural blanks were measured every 2 or 3 analyses in different sequences, and air-  
215 shots were measured every 8-12 hours to correct the instrumental mass discrimination. Gain between different collectors was  
216 monitored by measuring CO<sub>2</sub> on mass 44 in dynamic mode on all collectors. Gain was generally stable over periods of weeks.  
217 Note that because samples, standards and air calibration runs are measured during the same period, gain correction does not  
218 substantially change the final age results. The raw mass spectrometer data output was converted by an in-house designed Excel  
219 macro script to be compatible with the ArArCalc 2.5 data reduction software (Koppers, 2002). The  $^{40}\text{Ar}/^{36}\text{Ar}$  atmospheric air  
220 value of 298.56 from Lee et al. (2006) is used in the calculations. The correction factors for neutron interference reactions are  
221  $(2.64 \pm 0.02) \times 10^{-4}$  for  $(^{36}\text{Ar}/^{37}\text{Ar})_{\text{Ca}}$ ,  $(6.73 \pm 0.04) \times 10^{-4}$  for  $(^{39}\text{Ar}/^{37}\text{Ar})_{\text{Ca}}$ ,  $(1.21 \pm 0.003) \times 10^{-2}$  for  $(^{38}\text{Ar}/^{39}\text{Ar})_{\text{K}}$  and  $(8.6 \pm 0.7)$   
222  $\times 10^{-4}$  for  $(^{40}\text{Ar}/^{39}\text{Ar})_{\text{K}}$ . All uncertainties are quoted at the 1σ level and include all analytical errors (i.e. blank, mass  
223 discrimination and neutron interference correction and analytical error in J-factor, the parameter associated with the irradiation  
224 process).

225 A reliable plateau age is defined as experiments with at least 3 consecutive steps overlapping at 2-sigma, containing >50% of  
226 the  $^{39}\text{Ar}_{\text{K}}$ , a Mean Square Weighted Deviate (MSWD) value <2.5, and with a  $^{40}\text{Ar}/^{36}\text{Ar}$  inverse isochron intercept that does not  
227 deviate from atmospheric argon at 2-sigma. All the inverse isochron ages used the same steps as used in the weighted mean  
228 ages, and all relevant analytical data for the age calculations following standard practices (Schaen et al., 2020) can be found  
229 in supplementary material II.

## 230 2.3 Whole-rock major element analysis by XRF

231 Major-element concentrations were measured by X-ray fluorescence spectroscopy (XRF) on a Panalytical AxiosMax. A  
232 Panalytical Eagon2 was used to create 40mm fused glass beads of Li<sub>2</sub>B<sub>4</sub>O<sub>7</sub>/LiBO<sub>2</sub> (65.5:33.5%, Johnson & Johnson  
233 Spectroflux 110) with a 1:6 dilution sample-flux ratio that were molten at 1150 °C. Sample powders were ignited at 1000 °C



234 for 2 hours to determine loss on ignition (LOI) before being mixed with the  $\text{Li}_2\text{B}_4\text{O}_7/\text{LiBO}_2$  flux. Interference corrected spectra  
235 intensities were converted to oxide-concentrations against a calibration curve consisting of 30 international standards. The  
236 precision, expressed as the coefficient of variation (CV), is better than 0.5%. The accuracy, as measured on the international  
237 standards AGV-2, BHVO-2, BCR-2 and GSP-2 was better than 0.7% (1 RSD) (supplementary material III).

## 238 2.4 Eruption volume calculation

239 The minimum and/or maximum eruption volume of each volcano during each eruption period is derived from the ranges of  
240 thickness and surface areas that are reported in Campos and Rossi (1996) and Stewart and McPhie (2006). We converted these  
241 volumes to Dense Rock Equivalent (DRE) based on the magma type of different deposits. This analysis only includes the  
242 onshore deposits and results in a smaller estimate for larger pyroclastic volumes. The DRE volume is calculated using the  
243 equation of Crosweller et al. (2012):

$$244 \quad \text{DRE (km}^3\text{)} = \frac{\text{tephra vol (km}^3\text{)} \times \text{tephradensity (kg/m}^3\text{)}}{\text{magma density (kg/m}^3\text{)}}$$

245 Tephra density is assumed to be  $1000 \text{ kg/m}^3$  (Crosweller et al., 2012). Magma density varies depending on the magma type.  
246 Here we used  $2300 \text{ kg/m}^3$  for rocks with a  $\text{SiO}_2$  range of 65-77 wt.% and  $2500 \text{ kg/m}^3$  for all samples with  $\text{SiO}_2 < 65 \text{ wt.}\%$ .  
247 DRE corresponds to the unvesiculated erupted magma volume. Therefore, we did not convert the volume of some cryptodome  
248 and lavas from Profitis Illias (G15M0017), Triades (G15M0021-24), Dhemenehaki (G15M0032B) and Halepa (G15M0013)  
249 to the DRE since they contain less than 5% vesicles.

## 250 3 Results

### 251 3.1 $^{40}\text{Ar}/^{39}\text{Ar}$ age results

252 In this section, we present our groundmass, biotite and amphibole  $^{40}\text{Ar}/^{39}\text{Ar}$  results for eleven volcanic units of Milos. The  
253  $^{40}\text{Ar}/^{39}\text{Ar}$  ages range from 0.06 to 4.10 Ma and cover most of the major volcanic units of Milos. Table 2 and 3 show the  
254  $^{40}\text{Ar}/^{39}\text{Ar}$  results of incremental heating steps and single grain fusion analyses, respectively. Note that the Irr-ID column in  
255 these two Tables represents the irradiation ID of the analytical experiment (e.g. VU108-, VU110-) and the top right superscripts  
256 (G, B, A, O) in the sample IDs (e.g., G15M0029<sup>G</sup>, G15M0021<sup>B</sup>) refer to groundmass, biotite, amphibole and obsidian.

#### 257 3.1.1 Groundmass $^{40}\text{Ar}/^{39}\text{Ar}$ plateau and/or isochron ages

258 All groundmass samples yielding  $^{40}\text{Ar}/^{39}\text{Ar}$  plateau and isochron ages with more than 50%  $^{39}\text{Ar}_k$  and less than 2.5 MSWD  
259 included in their age spectrum are shown in Figure 4 and reported in Table 2. The  $^{40}\text{Ar}/^{36}\text{Ar}$  isochron intercepts do not deviate  
260 from atmospheric argon at the 2-sigma level, unless stated otherwise (Table 3). Sample G15M0016 was collected from a dyke  
261 at Kleftiko in the southwest of Milos (Figure 2). Three incremental heating experiments were performed on the groundmass  
262 of this sample (Figure 5A). The first experiment (VU108-Z8a) produced a weighted mean age of  $2.71 \pm 0.02 \text{ Ma}$  (MSWD  
263 2.31;  $^{39}\text{Ar}_k$  79.6%; inverse isochron age  $2.65 \pm 0.10 \text{ Ma}$ ). The other two, VU108-Z8a\_4 and VU108-Z8b\_1, have plateau ages  
264 of  $2.61 \pm 0.03 \text{ Ma}$  (MSWD 0.93;  $^{39}\text{Ar}_k$  57.4%; inverse isochron age  $2.69 \pm 0.10 \text{ Ma}$ ) and  $2.67 \pm 0.01 \text{ Ma}$  (MSWD 1.50;  $^{39}\text{Ar}_k$   
265 65.57%; inverse isochron age  $2.55 \pm 0.05 \text{ Ma}$ ), respectively. The three experiments are remarkably similar. Although the  
266 amount of radiogenic  $^{40}\text{Ar}$  is low (<20%), a combined age of  $2.66 \pm 0.01 \text{ Ma}$  is considered to be the best estimate with a  
267 relatively high MSWD value (2.51).

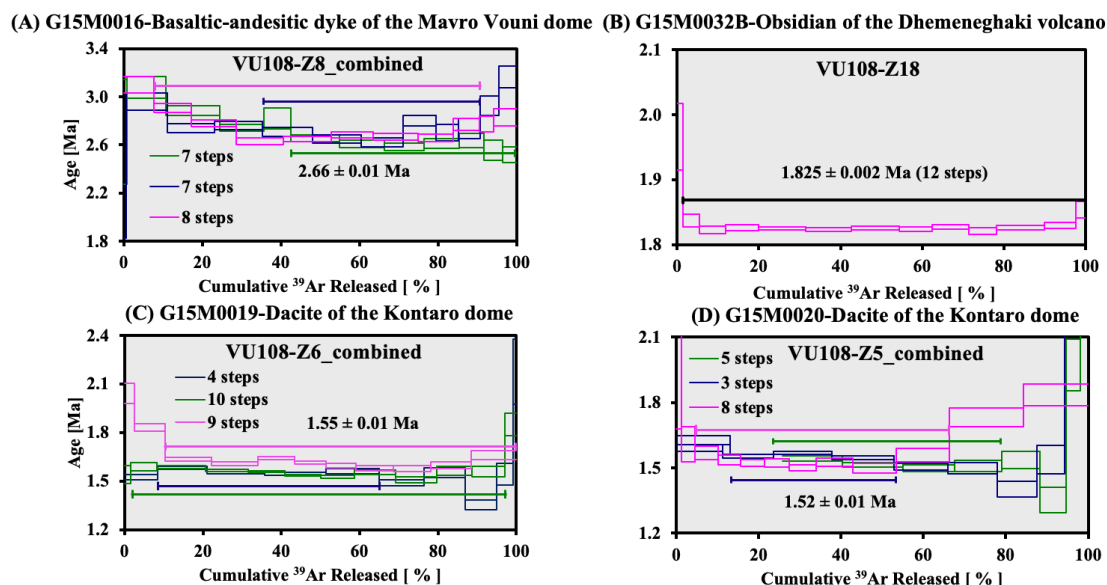


Figure 5. Groundmass  $^{40}\text{Ar}/^{39}\text{Ar}$  plateau ages for samples G15M0016 (A), G15M0032B (B), G15M0019 (C) and G15M0020 (D). The Mavro Vouni dome (A), Dhemeneghaki volcano (B) and Kontaro dacitic dome (C, D) are located in respectively the south-western, north-eastern and eastern parts of Milos VF (see Fig. 2). Final age calculation is reported with  $1\sigma$  errors. See the individual steps of sample G15M0016, G15M0019 and G15M0029 in supplementary material II.

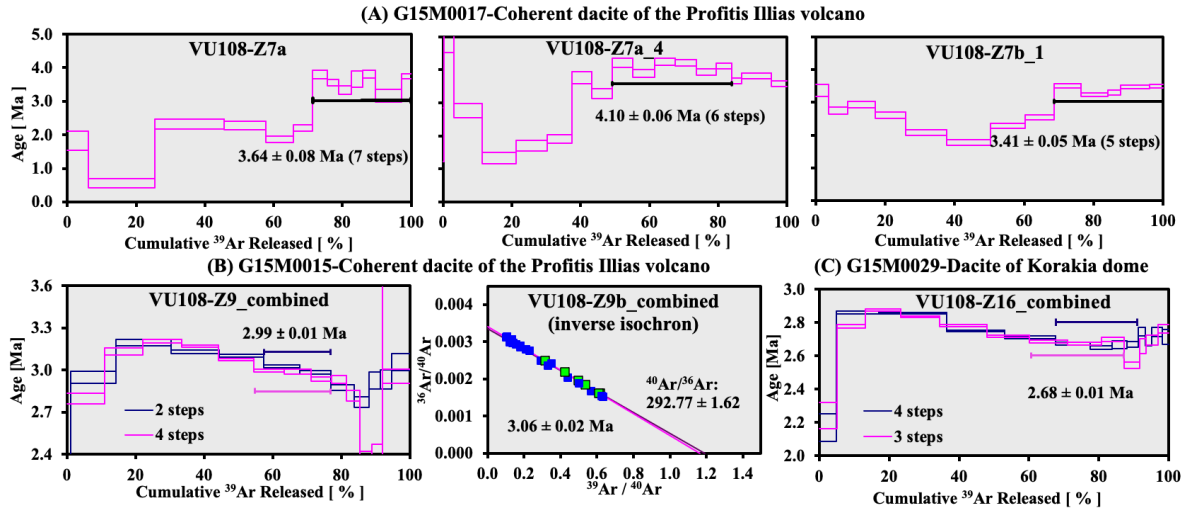
Two lava samples, G15M0019 and G15M0020, were collected from Kontaro in north-eastern Milos (Figure 2). Three replicate incremental heating step experiments on groundmass from sample G15M0019 (VU108-Z6a\_4; VU108-Z6a\_5 and VU108-Z6b\_1, Figure 5B) were performed that are not reproducible. Their plateau ages range from 1.55 Ma to 1.62 Ma with relatively high MSWD (3.8-4.5), 56-95% of the total  $^{39}\text{Ar}_K$ , 34-53% of radiogenic  $^{40}\text{Ar}$ , 0.88-1.02 of K/Ca and an atmospheric isochron intercept of 297-315. We consider the isochron age from the last experiment (VU108-Z6b\_1) as the reliable age ( $1.48 \pm 0.02$  Ma, MSWD 0.44) because its MSWD value is the only one smaller than 2.5 in this experiment, and therefore the best estimate for the eruption age. Three replicate incremental heating step experiments on groundmass from sample G15M0020 (VU108-Z5a\_5; VU108-Z5b\_1 and VU108-Z5b\_2, Figure 5C) were analysed. These experiments are similar at the lower temperature heating steps. They produced statistically meaningful plateau ages ranging from 1.52-1.56 Ma with 41-62% of the total  $^{39}\text{Ar}_K$ , 18-48% of radiogenic  $^{40}\text{Ar}$ , 1.51-1.73 of K/Ca and an atmospheric isochron intercept of 295-300. Their combined weighted mean age is  $1.54 \pm 0.01$  Ma (MSWD 3.06;  $^{39}\text{Ar}_K$  57.32%) with 25.31% of  $^{40}\text{Ar}^*$ .

Sample G15M0032B (obsidian) was collected from a pumice cone volcano at Demeneghaki (Figure 2). One incremental heating experiment on this sample (VU108-Z18, Figure 5D) yielded a plateau age of  $1.825 \pm 0.002$  Ma (MSWD 0.91;  $^{39}\text{Ar}_K$  98.6%). The  $^{40}\text{Ar}^*$  is 93.86%. The inverse isochron age is identical to the weighted mean plateau age of  $1.825 \pm 0.002$  Ma. The age of  $1.825 \pm 0.002$  Ma is considered the best estimate for the eruption age of the Demeneghaki obsidian.

### 3.1.2 Groundmass $^{40}\text{Ar}/^{39}\text{Ar}$ plateau and/or isochron ages (25-40% $^{39}\text{Ar}_K$ released)

The results shown in Figure 5 did not yield weighted mean plateau ages according to standard criteria including  $^{39}\text{Ar}_K > 50\%$ , but still provide some useful age information. Sample G15M0017 was collected from a cryptodome of the Profitis Illias volcano of southwestern Milos (Figure 2). Three replicate incremental heating experiments, VU108-Z7a, VU108-Z7a\_4 and VU108-Z7b\_1, have been performed on this sample which resulted in disturbed age spectra (Figure 6A). The consecutive lower temperature steps of all experiments define ages of  $< 2.5$  Ma, which is much younger than the ages of the submarine pyroclastic products of the lower series at Kleftiko and/or Profitis Illias (3.0-3.5 Ma, Fytikas et al., 1986 and Stewart and McPhie, 2006). At the consecutive higher temperature heating steps, these experiments yielded  $3.64 \pm 0.08$  Ma ( $^{40}\text{Ar}/^{36}\text{Ar}$  293.87  $\pm$  4.77; VU108-Z7a),  $4.10 \pm 0.06$  Ma ( $^{40}\text{Ar}/^{36}\text{Ar}$  298.44  $\pm$  15.51; VU108-Z7a\_4) and  $3.41 \pm 0.05$  Ma ( $^{40}\text{Ar}/^{36}\text{Ar}$  295.97  $\pm$  7.34; VU108-Z7b\_1). The total fusion and inverse isochron ages of the three experiments gave large ranges of 2.25-3.23 and 3.68-4.14 Ma, respectively, and none of these high temperature heating steps produced a statistical plateau (all MSWD  $> 2.0$ ).

299 The amount of radiogenic  $^{40}\text{Ar}$  of both the  $^{40}\text{Ar}/^{39}\text{Ar}$  result from our sample and the K-Ar age data from previous studies  
 300 (Fytikas et al., 1986) is rather low (<15%) for a sample of this age based on our laboratory experience. Therefore, the estimated  
 301 age range for the oldest volcanic products of the Milos VF should be confirmed by other dating techniques.



302  
 303 **Figure 6. Groundmass  $^{40}\text{Ar}/^{39}\text{Ar}$  plateau or inverse isochron ages for samples G15M0017 (A), G15M0015 (B) and G15M0029 (C).**  
 304 **Individual steps and final age calculation are reported with  $1\sigma$  errors. The Profitis Illias volcano (A, B) and dacitic Korakia dome**  
 305 **(C) are located in the south-western and north-eastern parts of Milos VF, respectively (Fig. 2). See the individual steps of sample**  
 306 **G15M0015 and G15M0029 in supplementary material II.**

307 Sample G15M0015 is also a cryptodome breccia from Profitis Illias (Figure 2). Two replicate incremental step heating  
 308 experiments were performed on the groundmass of this sample (VU108-Z9a and VU108-Z9b\_1, Figure 6B). Experiment  
 309 VU108-Z9a groundmass shows a disturbing age spectrum and ages increase from  $\sim 3$  Ma in the initial heating steps to  $\sim 3.2$   
 310 Ma, followed by a decrease to  $\sim 3$  Ma in the high temperature heating steps. The consecutive heating steps only exist at the  
 311 lower temperature steps yielding a “plateau” of  $3.12 \pm 0.02$  Ma (MSWD 9.07). Due to the excess argon ( $^{40}\text{Ar}/^{36}\text{Ar}$   $304.19 \pm$   
 312  $1.25$  comprising 43.07% of the released  $^{39}\text{Ar}_K$ ), the inverse isochron of  $3.06 \pm 0.02$  Ma (MSWD 0.01) is more reliable for this  
 313 analysis. The inverse isochron age of the second groundmass (VU108-Z9b\_1) is identical at  $3.04 \pm 0.02$  Ma (MSWD 1.14;  
 314  $^{39}\text{Ar}_K$  27.00%) and  $^{40}\text{Ar}/^{36}\text{Ar}$  of  $293.83 \pm 1.38$  obtained at high temperature steps. The two experiments are remarkably similar.  
 315 Although the sample does not formally fulfil the definition of a plateau age comprising  $>50\%$   $^{39}\text{Ar}_K$  released, a combined age  
 316 of  $3.06 \pm 0.02$  Ma (MSWD 1.14;  $^{39}\text{Ar}_K$  22.79%,  $^{40}\text{Ar}^*$  41.77%) most likely represents the eruption age. This  $^{40}\text{Ar}/^{36}\text{Ar}$  age is  
 317 consistent with the K-Ar age from the same lithology of  $3.08 \pm 0.08$  Ma (Fytikas et al. 1986).

318 Sample G15M0029 is an andesite collected from Korakia in the northeast of Milos (Figure 2). Two incremental heating  
 319 experiments (VU108-Z16a and VU108-Z16b\_1, Figure 6C) were performed on this sample. The two experiments are  
 320 remarkably similar and show a decreasing age from  $\sim 2.85$  Ma at the lower temperature heating steps to 2.65 Ma at the higher  
 321 temperatures. The higher temperature heating steps of both experiments yielded weighted mean plateau ages of  $2.67 \pm 0.01$   
 322 Ma (MSWD 0.96;  $^{39}\text{Ar}_K$  23.61%,  $^{40}\text{Ar}^*$  56.34%; inverse isochron age  $2.68 \pm 0.02$  Ma) and  $2.69 \pm 0.01$  Ma (MSWD 1.32;  
 323  $^{39}\text{Ar}_K$  27.08%,  $^{40}\text{Ar}^*$  55.78%; inverse isochron age  $2.67 \pm 0.03$  Ma). The isochron intercepts for both experiments are  
 324 atmospheric. The combined age of  $2.68 \pm 0.01$  Ma should be considered with caution due to the rather low amount of released  
 325  $^{39}\text{Ar}$  (23-28%).

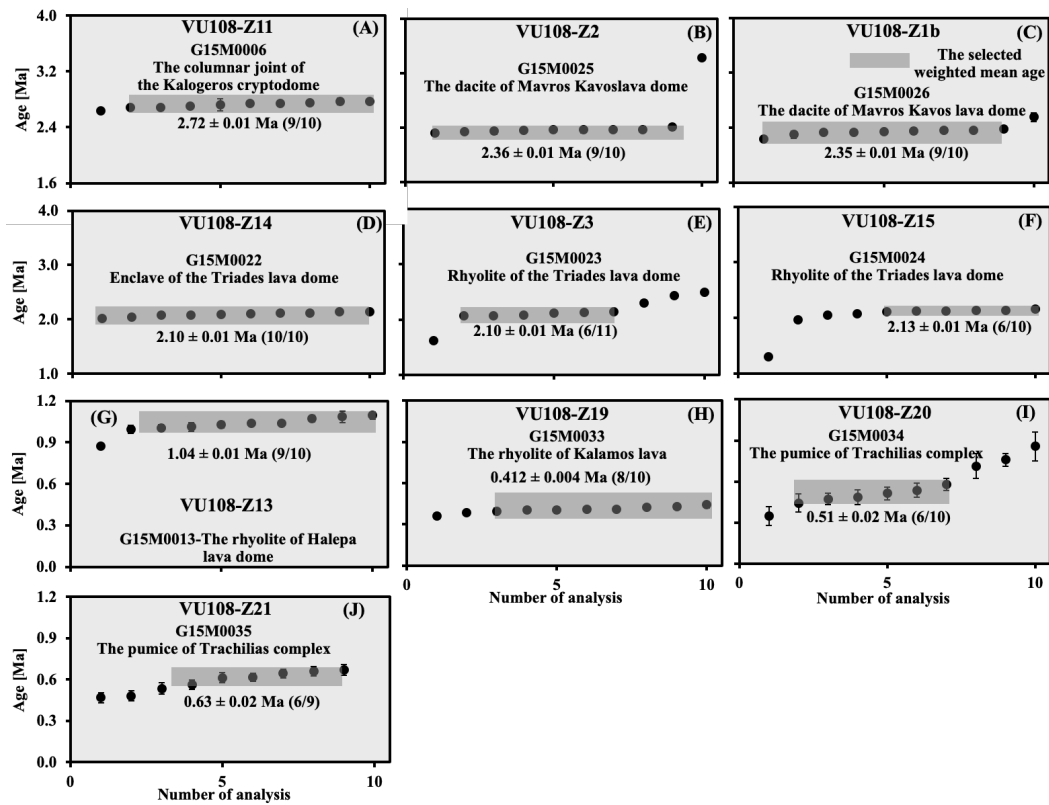


Figure 7. Biotite  $^{40}\text{Ar}/^{39}\text{Ar}$  total fusion ages for samples G15M0006 (A) and G15M0025-26(B, C), G15M0022-24 (D-F), G15M0013 (G) and G15M0033-35 (H-J). Data outside the shaded area are not included in the weighted mean. Individual steps and final age calculation are reported with  $1\sigma$  errors. The Kalogeros cryptodome and Mavros Kavos lava dome are located in the north-eastern and south-western parts of Milos VF, respectively, and Triades lava dome, Halepa lava dome, Trachilias complex and the Kalamos lava are situated in the southern, northern and south-eastern parts of Milos VF, respectively (see Fig. 2).

### 3.1.3 Single biotite grain $^{40}\text{Ar}/^{39}\text{Ar}$ fusion and/or isochron ages

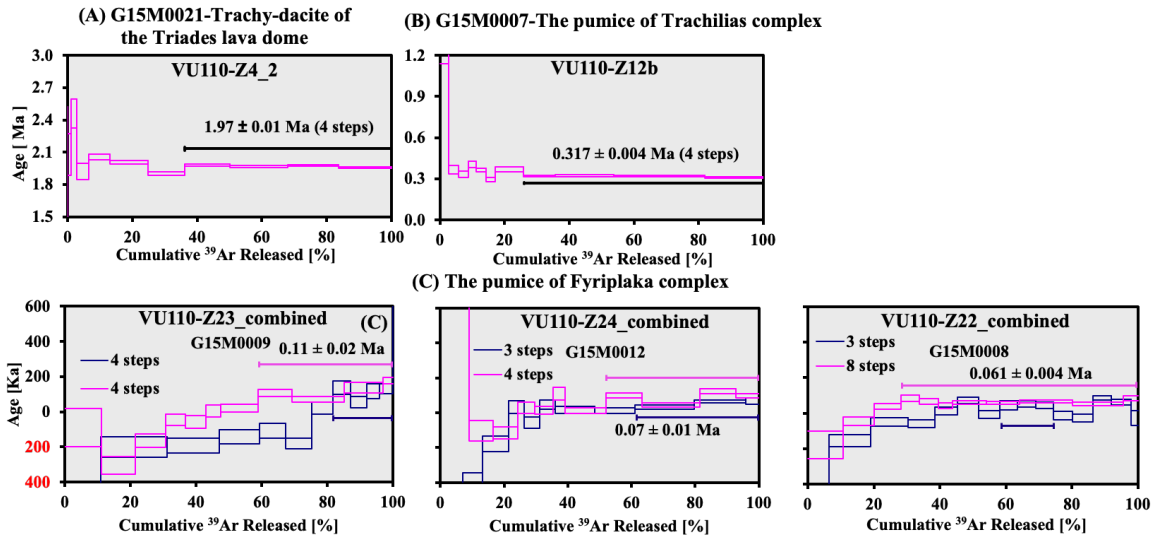
Results of nine single fusion experiments are given in Figure 7. Nine or ten replicate single fusion experiments were conducted on 5-10 grains biotite per fusion. Sample G15M0006 is from dacite with columnar joints from the Kalogeros cryptodome in the northeast of Milos (VU108-Z11, Figure 7A). The sample shows a weighted mean age of  $2.72 \pm 0.01$  Ma for 9 out of 10 total fusion experiments (MSWD 1.95; 9/10) with an average 47.9% of radiogenic  $^{40}\text{Ar}$ . The inverse isochron age is  $2.62 \pm 0.04$  Ma (MSWD 0.99). Note that excess argon ( $^{40}\text{Ar}/^{36}\text{Ar}$   $310.2 \pm 4.0$ ) is present. Hence the inverse isochron age is younger compared to the weighted mean age. The isochron age of  $2.62 \pm 0.04$  Ma is considered as the best estimate for the emplacement age.

Sample G15M0025 was collected from the Mavros Kavos lava dome located in the west of Milos (Figure 2). The biotite of this sample (VU108-Z2, Figure 7B) shows a weighted mean age of  $2.36 \pm 0.01$  Ma (MSWD 0.70; 9/10;  $^{40}\text{Ar}^*$  37.60%, inverse isochron age  $2.34 \pm 0.04$  Ma) with an  $^{40}\text{Ar}/^{36}\text{Ar}$  intercept of  $300.6 \pm 3.5$ . The age of  $2.36 \pm 0.01$  Ma is considered the best eruption age estimate for this sample.

Sample G15M0023 and G15M0024 are from the Triades lava dome northeast of Milos (Figure 2). A mafic enclave G15M0022 (host rock G15M0021) was collected from a lava near Cape Vani (Figure 2). The total fusion experiments of the biotites show that their initial  $^{40}\text{Ar}/^{36}\text{Ar}$  estimates overlap with air (296-300). The total fusion ages gave the best estimates for their eruption ages of 2.10-2.13 Ma using 22 out of 31 fusions with a range of radiogenic  $^{40}\text{Ar}$  between 30-36% (Figure 7B).

Sample G15M0013 is from the rhyolitic Halepa lava dome in the south of Milos (Figure 2). The total fusion experiment (VU108-Z13, Figure 7C) on biotite of this sample produced a weighted mean age of  $1.04 \pm 0.01$  Ma (MSWD 1.62; 9/10,  $^{40}\text{Ar}^*$  26.3%; inverse isochron age  $1.02 \pm 0.04$  Ma) with an initial  $^{40}\text{Ar}/^{36}\text{Ar}$  estimate of  $299.8 \pm 4.1$ . The best estimate for the eruption age of the Halepa rhyolite is  $1.04 \pm 0.01$  Ma.

352 Sample G15M0034 and G15M0035 were collected from a lava dome located southeast of the Trachilas cone (Figure 2). Nine  
 353 total fusion experiments (VU108-Z21, Figure 7C) were performed on biotite of sample G15M0035 and yielded the age of  $0.63 \pm 0.02$  Ma (MSWD 1.26; 6/9;  $^{40}\text{Ar}^*$  4.9%; inverse isochron age  $0.77 \pm 0.13$  Ma). The atmospheric isochron intercept overlaps  
 354 with air at 2-sigma ( $296.4 \pm 1.7$ ). The 4.9% of radiogenic  $^{40}\text{Ar}$  is so low that we should consider the age of  $0.63 \pm 0.02$  Ma  
 355 with caution. For biotite of sample G15M0034 (VU108-Z20, Figure 7C) one total fusion experiment produced a weighted  
 356 mean age of  $0.51 \pm 0.02$  Ma (MSWD 0.95; 6/10;  $^{40}\text{Ar}^*$  3.5%; inverse isochron age  $0.61 \pm 0.08$  Ma) with an atmospheric  
 357 isochron intercept. The age of  $0.51 \pm 0.02$  Ma also needs to be considered as possibly suspect due to the low amount of  
 358 radiogenic  $^{40}\text{Ar}$ .  
 359



360  
 361 **Figure 8. Biotite  $^{40}\text{Ar}/^{39}\text{Ar}$  plateau ages for samples G15M0021 (A), G15M0007 (B), and G15M0009 (VU110-Z23\_combined),**  
 362 **G15M0012 (VU110-Z24\_combined) and G15M0008 (VU110-Z22\_combined) (C). The numbers in red represent negative ages.**  
 363 **Individual steps and final age calculation are reported with  $1\sigma$  errors. The Triades lava dome, Trachilas and Fyriplaka complexes**  
 364 **are located in the north-western, northern and south-eastern parts of Milos VF, respectively (see Fig. 2). See the individual steps of**  
 365 **sample G15M0021, G15M0007, G15M0009, G15M0012 and G15M0008 in supplementary material II.**

366 Sample G15M0033 was collected from the Kalamos lava along the coast of the southwest of the Fyriplaka rhyolitic complex  
 367 (Figure 2). Biotite of this sample (VU108-Z19, Figure 7C) yielded  $0.412 \pm 0.004$  Ma (MSWD 1.10; 8/10; inverse isochron  
 368 age  $0.39 \pm 0.02$  Ma) with  $\sim 22.2\%$  of radiogenic  $^{40}\text{Ar}$  which is considered as the eruption age for the Kalamos lava.

### 369 3.1.4 Multiple biotite grain $^{40}\text{Ar}/^{39}\text{Ar}$ incremental heating plateau and/or isochron ages

370 Figure 8 displays the biotite  $^{40}\text{Ar}/^{39}\text{Ar}$  ages measured by the incremental heating steps method. Sample G15M0021 is the host  
 371 lava of mafic enclave G15M0022. Twelve replicate total fusion experiments on its biotite (VU110-Z4, Table 3) produced an  
 372 age of  $2.48 \pm 0.04$  Ma (MSWD 1.49; 4/12,  $^{40}\text{Ar}^*$  36.09%; inverse isochron age  $3.44 \pm 0.46$  Ma). Although this suggests a  
 373 correct age, the large analytical error of each fusion ( $>0.3$  Ma on average) and poor reproducibility (4/12) of this experiment  
 374 probably results in an unreliable age. Therefore, two more incremental heating experiments were performed on this sample  
 375 (VU110-Z4\_2 and VU110-Z4\_2b, Figure 8A), that gave an age of  $1.97 \pm 0.01$  Ma (MSWD 1.66;  $^{39}\text{Ar}_K$  63.8%,  $^{40}\text{Ar}^*$  54.7%;  
 376 inverse isochron age  $1.97 \pm 0.03$  Ma) and  $2.01 \pm 0.01$  Ma (MSWD 6.76;  $^{39}\text{Ar}_K$  75.39%,  $^{40}\text{Ar}^*$  57.84%; inverse isochron age  
 377  $2.04 \pm 0.05$  Ma), respectively. The scatter in the latter is too high to define a reliable plateau age and the first incremental  
 378 heating experiment is considered as the best estimate of the eruption age of this sample.

379 Sample G15M0007 was collected from the rhyolitic Trachilas complex in the north of Milos (Figure 2). Twenty-two total  
 380 fusion (VU110-Z12, Table 3) and two incremental heating experiments (VU110-Z12a and 12b, Figure 8B) were performed  
 381 on biotite of this sample. The total fusion experiments did not result in a reliable age due to the large errors of single steps ( $\pm$   
 382  $0.19$  Ma on average) and the rather low amount of radiogenic  $^{40}\text{Ar}$  (9.1%). On the other hand, the first incremental heating  
 383 experiment produced a plateau age of  $0.30 \pm 0.01$  Ma (MSWD 4.61;  $^{39}\text{Ar}_K$  56.60%; inverse isochron age  $0.28 \pm 0.05$  Ma)  
 384 including 14.51% of radiogenic  $^{40}\text{Ar}$ . The second incremental heating experiment yielded a plateau of  $0.317 \pm 0.004$  Ma

385 (MSWD 1.29;  $^{39}\text{Ar}_K$  74.05%; inverse isochron age  $0.31 \pm 0.03$  Ma) with a higher amount of radiogenic  $^{40}\text{Ar}$  (18.30%). The  
 386 isochron intercepts of both incremental heating experiments are atmospheric. The second experiment is the best estimate for  
 387 the eruption age, since it contained the largest amount of radiogenic  $^{40}\text{Ar}$  and has a better reproducibility of single heating  
 388 steps.

389 Three pumice clasts (G15M0008-9 and G15M0012) were sampled from different layers of the Fyriplaka complex (Figure 2).  
 390 The first incremental step heating experiment on biotite from sample G15M0009 (VU110-Z23a, Figure 8C) gave negative  
 391 ages at the lower temperature heating steps. Four consecutive higher temperature heating steps seem to define a “plateau” of  
 392  $0.11 \pm 0.02$  Ma (MSWD 1.37) only using 18.33% of the total  $^{39}\text{Ar}_K$  with 1.65% of radiogenic  $^{40}\text{Ar}$ . The second experiment  
 393 (VU110-Z23b) also yielded a “plateau” of  $0.11 \pm 0.03$  Ma (MSWD 6.77) at higher temperature heating steps including 41.05%  
 394 of the total  $^{39}\text{Ar}_K$  and 3.13% of radiogenic  $^{40}\text{Ar}$ . The significantly larger error of the isochron age may be due to the clustering  
 395 of data close to zero on the y-axis. The two experiments (VU110-Z23a and Z23b) are comparable. The combined age of  $0.11$   
 396  $\pm 0.02$  (MSWD 3.5) is consistent with the age of 0.09-0.14 Ma from Fytikas et al. (1986). Although only 29.50% of the released  
 397  $^{39}\text{Ar}_K$  was used for this sample, we believe this age is the eruption age of this layer in the Fyriplaka complex.

398 For biotite of sample G15M0012, both incremental step heating experiments are comparable. Both of them yielded plateau  
 399 ages of  $0.05 \pm 0.01$  Ma (VU110-Z24a; MSWD 3.09;  $^{39}\text{Ar}_K$  38.89%,  $^{40}\text{Ar}^*$  2.89%; inverse isochron age  $0.14 \pm 0.03$  Ma) and  
 400  $0.09 \pm 0.02$  Ma (VU110-Z24b; MSWD 8.16;  $^{39}\text{Ar}_K$  48.04%,  $^{40}\text{Ar}^*$  4.59%; inverse isochron age  $0.09 \pm 0.05$  Ma) at higher  
 401 temperature heating steps (Figure 8C). The clustering of data points of experiment VU110-Z24a could result in the lower  
 402 initial estimate of  $^{40}\text{Ar}/^{36}\text{Ar}$  ( $285.98 \pm 4.76$ ). However, the combined age of  $0.07 \pm 0.01$  Ma, using 43.53% of the total  $^{39}\text{Ar}_K$   
 403 with an atmospheric isochron intercept ( $295.67 \pm 7.39$ ), could be the representative age of eruption.

404 Biotite of sample G15M0008 did not result in a reliable plateau in the first incremental step heating experiment (VU110-Z22a,  
 405 Figure 8C) but shows a very disturbed age spectrum. The second experiment (VU110-Z22b) yielded  $0.062 \pm 0.003$  Ma (MSWD  
 406 0.91) using 71.81% of the total  $^{39}\text{Ar}_K$  with 2.69% of radiogenic  $^{40}\text{Ar}$  as the best estimate of the eruption age.

### 407 3.1.5 Multiple amphibole grain $^{40}\text{Ar}/^{39}\text{Ar}$ multi-grain incremental heating plateau and/or isochron ages

408 There are only two amphibole samples that yielded  $^{40}\text{Ar}/^{36}\text{Ar}$  plateau and/or isochron ages (Figure 9A and B). Sample  
 409 G15M0004 was collected from the pyroclastic series of Adamas from the PSLD (Fytikas et al., 1986), to the north of Bombarda  
 410 (Figure 2). Two replicate heating experiments of G15M0004 amphibole (VU108-Z10\_1 and VU108-Z10\_2) were performed

411 **Table 2. Incremental heating  $^{40}\text{Ar}/^{39}\text{Ar}$  results of the Milos volcanic field.**

Volcanic Unit	Sample -ID	Irr-ID	Latitude	Age $\pm 1\sigma$ (Ma)	MS WD	$^{39}\text{Ar}_K$ (%)	n/ntotal	$^{40}\text{Ar}^*$ (%)	K/Ca $\pm 1\sigma$	Inverse isochron age (Ma)	$^{40}\text{Ar}/^{36}\text{Ar} \pm 1\sigma$	MS WD
Fyriplaka Complex	G15 M00 08 <sup>B</sup>	VU110-Z22a	36.67 29 N	$0.05 \pm 0.01$	0.04	16.24	3/15	1.20	$60.9 \pm 10.6$	$0.05 \pm 0.10$	$298.08 \pm 8.77$	0.08
		VU110-Z22b	24.46	<b><math>0.062 \pm 0.003</math></b>	0.91	71.81	8/11	2.69	$57.3 \pm 8.4$	$0.06 \pm 0.02$	$299.39 \pm 3.66$	1.09
		Combined (Z22)	70 E	$0.061 \pm 0.004$	0.82	41.37	11/26	2.29	$58.0 \pm 6.3$	$0.07 \pm 0.01$	$296.78 \pm 1.78$	0.83
	G15 M00 12 <sup>B</sup>	VU110-Z24a	36.67 95 N	$0.05 \pm 0.01$	3.09	38.89	3/11	2.89	$40.0 \pm 6.0$	$0.14 \pm 0.03$	$285.98 \pm 4.76$	0.07
		VU110-Z24b	24.48	$0.09 \pm 0.02$	8.16	48.04	4/11	4.59	$30.1 \pm 7.1$	$0.09 \pm 0.05$	$297.46 \pm 10.29$	12.78
		Combined(Z24)	28 E	<b><math>0.07 \pm 0.01</math></b>	7.44	43.53	7/22	3.86	$32.3 \pm 5.0$	$0.09 \pm 0.03$	$295.67 \pm 7.39$	9.02
	G15 M00 09 <sup>B</sup>	VU110-Z23a	36.67 16 N	$0.11 \pm 0.02$	1.37	18.33	4/12	1.65	$45.4 \pm 7.3$	$0.76 \pm 0.30$	$268.52 \pm 17.08$	0.90
		VU110-Z23b	24.48	$0.11 \pm 0.03$	6.77	41.05	4/11	3.13	$19.4 \pm 3.7$	$0.29 \pm 0.14$	$285.17 \pm 15.80$	8.09
		Combined (Z23)	91 E	<b><math>0.11 \pm 0.02</math></b>	3.50	29.50	8/21	2.39	$19.7 \pm 2.6$	$0.15 \pm 0.05$	$295.78 \pm 4.34$	4.04
Trachilas Complex	G15 M00 07 <sup>B</sup>	VU110-Z12a	36.76 71 N	$0.30 \pm 0.01$	4.61	56.50	8/16	14.51	$38.3 \pm 2.4$	$0.28 \pm 0.05$	$301.42 \pm 9.01$	5.47
		VU110-Z12b	24.41	<b><math>0.317 \pm 0.004</math></b>	1.29	74.05	4/11	18.30	$32.0 \pm 2.5$	$0.31 \pm 0.03$	$299.52 \pm 6.40$	2.04
		Combined (Z12)	24 E	$0.31 \pm 0.01$	5.57	65.27	12/27	15.77	$33.1 \pm 1.6$	$0.34 \pm 0.03$	$293.05 \pm 5.50$	5.84
Kontaro dome		VU108-Z5a_5	36.72 34 N	$1.52 \pm 0.01$	1.06	61.82	8/12	18.30	$1.51 \pm 0.05$	$1.49 \pm 0.02$	$300.03 \pm 0.86$	0.95
		VU108-Z5b_1		$1.56 \pm 0.01$	1.94	41.54	3/10	47.94	$1.73 \pm 0.06$	$1.58 \pm 0.02$	$294.97 \pm 3.74$	2.17

	G15 M00 20 <sup>G</sup>	VU108-Z5b_2 Combined (Z5)	24.39 52 E	1.52 ± 0.01	1.73	62.45	5/10	22.95	1.56 ± 0.08	1.53 ± 0.02	298.12 ± 0.89	2.34
				<b>1.54 ± 0.01</b>	3.06	57.32	16/32	25.31	1.58 ± 0.04	1.55 ± 0.01	297.41 ± 0.57	2.82
	G15 M00 19 <sup>G</sup>	VU108-Z6a_4 VU108-Z6a_5 VU108-Z6b_1 Combined (Z6)	36.72 11 N 24.39 50 E	1.62 ± 0.01	3.80	89.75	9/11	34.28	0.91 ± 0.05	1.62 ± 0.02	297.66 ± 1.36	4.40
				1.55 ± 0.01	4.50	95.41	10/12	35.26	0.88 ± 0.06	1.55 ± 0.01	298.73 ± 1.29	5.40
				1.56 ± 0.01	4.05	56.64	4/10	53.19	1.02 ± 0.01	<b>1.48 ± 0.02</b>	315.46 ± 5.20	0.44
				1.55 ± 0.01	32.15	80.97	27/45	38.78	0.93 ± 0.04	1.53 ± 0.02	300.60 ± 2.27	34.25
Dheme- neghaki volcano	G15 M00 32B <sup>O</sup>	VU108-Z18	36.70 84 N 24.53 24 E	<b>1.825 ± 0.002</b>	0.91	98.64	12/13	93.86	1.83 ± 0.04	1.825 ± 0.003	301.52 ± 3.34	0.93
Triades lava dome	G15 M00 21 <sup>B</sup>	VU110-Z4_2 VU110-Z4_2b Combined (Z4)	36.74 02 N 24.33 97 E	<b>1.97 ± 0.01</b>	1.66	63.83	4/12	54.72	107.55 ± 20.64	1.97 ± 0.03	299.16 ± 5.36	2.56
				2.01 ± 0.01	6.76	75.39	6/16	57.84	54.43 ± 8.29	2.04 ± 0.05	293.08 ± 10.44	8.15
				1.99 ± 0.01	9.08	69.12	10/28	56.59	73.52 ± 6.46	2.00 ± 0.04	295.64 ± 7.89	10.30
Adamas lava dome	G15 M00 04 <sup>A</sup>	VU108-Z10_1 VU108-Z10_2 Combined (Z10)	36.72 82 N 24.43 15 E	2.99 ± 0.11	1.00	87.31	4/12	16.36	0.030 ± 0.002	7.89 ± 2.46	202.39 ± 48.47	0.01
				2.86 ± 0.09	1.50	86.18	7/11	17.58	0.029 ± 0.002	0.70 ± 0.29	348.91 ± 27.33	1.00
				2.90 ± 0.07	1.31	86.74	11/23	17.13	0.029 ± 0.001	<b>1.95 ± 0.45</b>	319.51 ± 14.70	1.17
The dyke of Mavro Vouni lava dome	G15 M00 16 <sup>G</sup>	VU108-Z8a VU108-Z8a_4 VU108-Z8b_1 Combined (Z8)	36.66 68 N 24.33 98 E	2.71 ± 0.02	2.31	79.64	8/12	16.57	0.24 ± 0.05	2.65 ± 0.10	299.84 ± 2.32	2.92
				2.61 ± 0.03	0.93	57.41	7/12	16.86	0.12 ± 0.07	2.69 ± 0.10	296.44 ± 2.49	0.69
				2.67 ± 0.01	1.50	65.57	7/11	17.25	0.11 ± 0.04	2.55 ± 0.05	301.53 ± 1.14	0.71
				<b>2.66 ± 0.01</b>	2.51	67.27	22/35	16.87	0.14 ± 0.02	2.61 ± 0.05	300.01 ± 1.18	2.78
Korokia dome	G15 M00 29 <sup>G</sup>	VU108-Z16a VU108-Z16b_1 Combined (Z16)	36.74 65 N 24.52 00 E	2.67 ± 0.01	0.96	23.61	4/13	56.34	0.53 ± 0.05	2.68 ± 0.02	296.64 ± 3.18	1.25
				2.69 ± 0.01	1.32	27.08	3/13	55.78	0.55 ± 0.04	2.67 ± 0.03	301.16 ± 4.72	2.13
				2.68 ± 0.01	1.66	25.30	7/26	56.10	0.54 ± 0.03	2.67 ± 0.02	300.00 ± 2.94	1.98
Coherent dacite of Profitis Ilias volcano	G15 M00 15 <sup>G</sup>	VU108-Z9a VU108-Z9b_1 Combined (Z9)	36.66 29 N 24.35 96 E	3.12 ± 0.02	9.07	43.07	3/12	42.73	1.31 ± 0.05	3.06 ± 0.02	304.19 ± 1.25	0.01
				2.98 ± 0.02	4.53	27.00	4/14	39.35	0.98 ± 0.06	3.04 ± 0.02	293.83 ± 1.38	1.14
				2.99 ± 0.02	5.54	22.79	6/26	41.77	1.00 ± 0.04	<b>3.06 ± 0.02</b>	292.77 ± 1.62	1.90
Coherent dacite of Profitis Ilias volcano	G15 M00 17 <sup>G</sup>	VU108-Z7a VU108-Z7a_4 VU108-Z7b_1 Combined (Z7)	36.65 96 N 24.36 75 E	<b>3.64 ± 0.08</b>	3.13	28.62	7/13	9.77	1.04 ± 0.02	4.14 ± 0.49	293.87 ± 4.77	3.44
				<b>4.10 ± 0.06</b>	2.13	34.71	6/17	9.08	1.10 ± 0.01	4.11 ± 1.40	298.44 ± 15.51	3.24
				<b>3.41 ± 0.05</b>	3.95	31.41	5/13	9.95	1.00 ± 0.03	3.68 ± 0.71	295.97 ± 7.34	7.09
				3.63 ± 0.08	14.04	31.40	18/43	9.59	1.04 ± 0.02	2.19 ± 0.32	311.31 ± 3.60	10.19

412 The age in bold is considered as the best estimate of the eruptive age.

413 The <sup>40</sup>Ar\* (%) is the average radiogenic <sup>40</sup>Ar of the analyses included in the weighted mean.

414 The experiment was analyzed on biotite<sup>B</sup>, obsidian<sup>O</sup>, amphibole<sup>A</sup> and groundmass<sup>G</sup> of a sample.

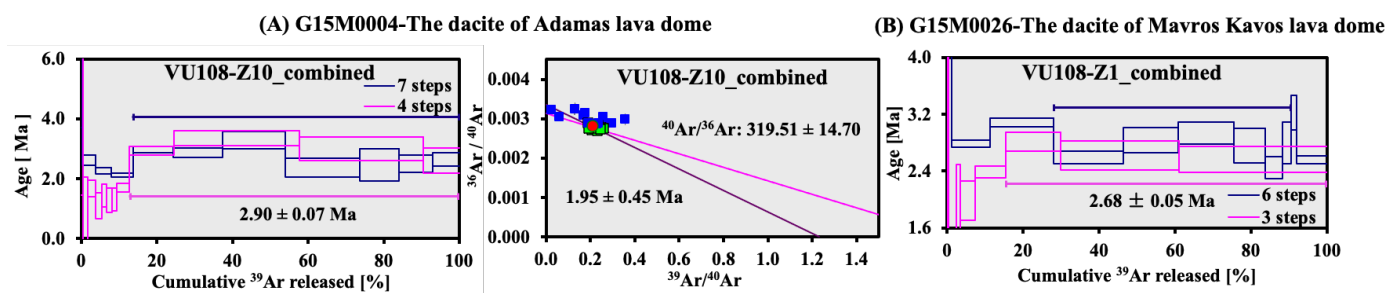
415 The same steps were used for the calculation of isochron ages as used in the weighted mean ages.

416 **Table 3. <sup>40</sup>Ar/<sup>39</sup>Ar results of single grain fusion analyses on the Milos volcanic field.**

Volcanic unit	Sample-ID	Irr-ID	Location	Age ± 1σ (Ma)	MS WD	<sup>39</sup> Ar <sub>K</sub> (%)	n/ntotal	<sup>40</sup> Ar* (%)	K/Ca ± 1σ	Inverse isochron age (Ma)	<sup>40</sup> Ar/ <sup>36</sup> Ar ± 1σ	MS WD
Fyriplaka complex	G15M0008 <sup>B</sup>	VU11 0-Z22	36.6729 N 24.4670 E	0.71 ± 0.06	0.41	25.78	8/23	8.67	17.5 ± 1.8	0.64 ± 0.20	302.75 ± 12.62	0.46
	G15M0012 <sup>B</sup>	VU11 0-Z24	36.6795 N 24.4828 E	1.12 ± 0.11	2.26	60.49	14/23	7.32	14.9 ± 0.8	0.26 ± 0.07	316.75 ± 19.49	2.29
	G15M0009 <sup>B</sup>	VU11 0-Z23	36.6716 N 24.4891 E	0.65 ± 0.07	1.16	79.91	19/23	5.87	12.0 ± 0.5	0.28 ± 0.07	309.57 ± 16.01	1.22
Trachilas complex	G15M0007 <sup>B</sup>	VU11 0-Z12	36.7671 N 24.4124 E	0.47 ± 0.05	0.75	72.65	15/22	9.09	14.8 ± 0.5	0.55 ± 0.12	293.95 ± 11.30	0.80
Kalamos lava	G15M0033 <sup>B</sup>	VU10 8-Z19	36.6662 N 24.4652 E	<b>0.412 ± 0.004</b>	1.10	77.24	8/10	22.22	20.5 ± 2.7	0.39 ± 0.02	303.32 ± 3.06	0.89
Trachilas complex	G15M0034 <sup>B</sup>	VU10 8-Z20	36.7550 N 24.4244 E	<b>0.51 ± 0.02</b>	0.95	56.92	6/10	3.53	13.7 ± 1.2	0.61 ± 0.08	296.45 ± 1.65	0.92
	G15M0035 <sup>B</sup>	VU10 8-Z21	36.7550 N 24.4244 E	<b>0.63 ± 0.02</b>	1.26	73.43	6/9	4.87	17.7 ± 1.1	0.77 ± 0.13	294.99 ± 3.17	1.42
Halepa lava dome	G15M0013 <sup>B</sup>	VU10 8-Z13	36.6716 N 24.4406 E	<b>1.04 ± 0.01</b>	1.62	82.40	9/10	26.30	*15.2 ± 0.2	1.02 ± 0.04	299.77 ± 4.06	0.00

Triades lava dome	G15M0021 <sup>B</sup>	VU11 0-Z4	36.7402 N 24.3397 E	<b>2.48 ± 0.04</b>	1.49	87.08	4/12	36.09	13.00± 0.60	3.44 ± 0.46	228.58 ± 36.66	1.39
	G15M0022 <sup>B</sup>	VU10 8-Z14	36.7402 N 24.3397 E	<b>2.10 ± 0.01</b>	1.37	100.0 0	10/10	36.04	*11.7 ± 0.2	2.08 ± 0.06	299.44 ± 4.63	1.59
	G15M0023 <sup>B</sup>	VU10 8-Z3	36.7263 N 24.3420 E	<b>2.10 ± 0.01</b>	1.72	55.58	6/11	35.93	*76.1 ± 2.4	2.13 ± 0.06	296.12 ± 4.63	2.08
	G15M0024 <sup>B</sup>	VU10 8-Z15	36.7277 N 24.3415 E	<b>2.13 ± 0.01</b>	0.46	63.67	6/10	29.74	22.5 ± 3.2	2.09 ± 0.03	300.50 ± 1.58	0.23
Mavros Kavos lava dome	G15M0025 <sup>B</sup>	VU10 8-Z2	36.6876 N 24.3515 E	<b>2.36 ± 0.01</b>	0.70	84.62	9/10	37.62	43.2 ± 2.7	2.34 ± 0.04	300.57 ± 3.49	0.78
	G15M0026 <sup>B</sup>	VU10 8-Z1b	36.6848 N 24.3500 E	2.35 ± 0.01	1.36	95.23	9/10	38.56	12.8 ± 2.3	<b>2.42 ± 0.04</b>	292.01 ± 2.92	0.93
Kalegero scrypto- dome	G15M0006 <sup>B</sup>	VU10 8-Z11	36.7643 N 24.5157 E	2.72 ± 0.01	1.95	87.67	9/10	47.90	*28.3 ± 0.5	<b>2.62 ± 0.04</b>	310.21 ± 4.04	0.99

417 The age in bold is considered as the best estimate of the eruptive age.  
418 The <sup>40</sup>Ar\* (%) is the average radiogenic <sup>40</sup>Ar of the analyses included in the weighted mean.  
419 \*The K/Ca ratio is calibrated by removing the total fusion with excess <sup>37</sup>Ar (Ca) (fA>1).  
420 <sup>B</sup>The experiment was analyzed on biotite of the sample.  
421 The same steps were used for the calculation of isochron ages as used in the weighted mean ages.

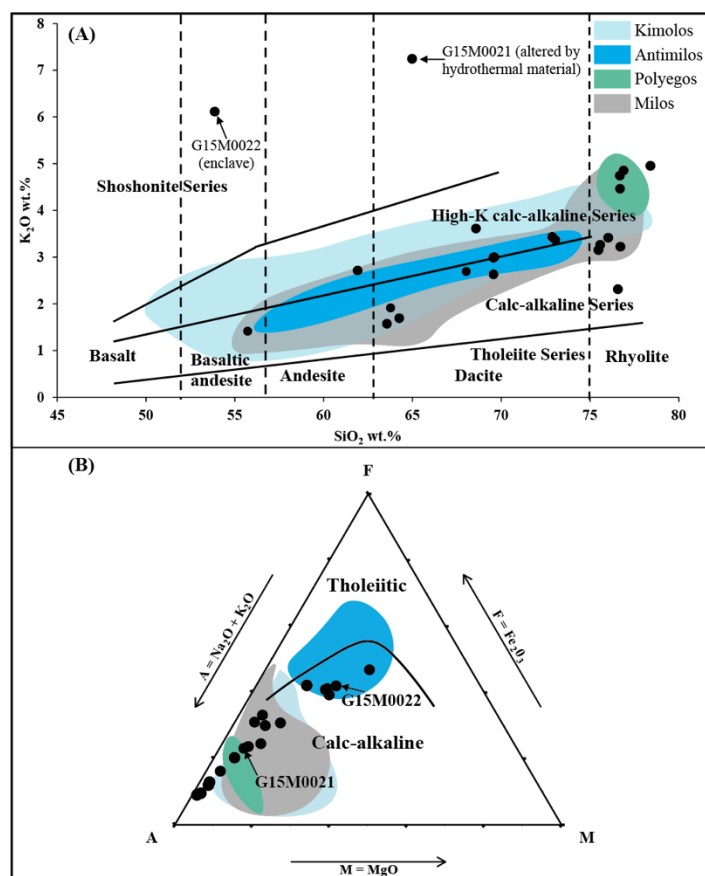


422 **Figure 9. Amphibole <sup>40</sup>Ar/<sup>39</sup>Ar plateau or inverse isochron ages for samples G15M0004 (A) and G15M0026 (B). Final age**  
423 **calculation is reported with 1σ errors. The Adamas and Mavros Kavos lava domes are located in the northern and south-western**  
424 **parts of Milos VF, respectively (see Fig. 2). See the individual steps of sample G15M0004 and G15M0026 in supplementary**  
425 **material II.**

427 yielding 2.99 ± 0.11 Ma (MSWD 1.00; <sup>39</sup>Ar<sub>K</sub> 87.31%, <sup>40</sup>Ar\* 16.36%; inverse isochron age 7.89 ± 2.46 Ma) and 2.86 ± 0.09  
428 Ma (MSWD 1.50; <sup>39</sup>Ar<sub>K</sub> 86.18%, <sup>40</sup>Ar\* 17.58%; inverse isochron age 0.70 ± 0.29 Ma). The variable atmospheric isochron  
429 intercept of both experiments (<sup>40</sup>Ar/<sup>36</sup>Ar 202.39 ± 48.47 and 348.91 ± 27.33) is due to the clustering of the data points. Note  
430 that also the amount of radiogenic <sup>40</sup>Ar is rather low (~17%). The two experiments are remarkably similar. A combined inverse  
431 isochron age of 1.95 ± 0.45 Ma (MSWD 1.17; <sup>40</sup>Ar/<sup>36</sup>Ar 319.51 ± 14.70) is considered the best estimate, but ideally this age  
432 should be checked by other techniques.

433 Sample G15M0026 is from the same location as sample G15M0025, which gives us the opportunity to compare the biotite age  
434 with the amphibole age. One total fusion experiment on biotite (VU108-Z1b) yielded a weighted mean age of 2.35 ± 0.01 Ma  
435 (MSWD 1.36; <sup>40</sup>Ar\* 38.6%). The atmospheric isochron intercept is low (<sup>40</sup>Ar/<sup>36</sup>Ar 292.01 ± 2.92), the inverse isochron age of  
436 2.42 ± 0.04 Ma (MSWD 0.93) is considered the best result from the biotite. Two incremental heating experiments for  
437 amphibole (VU108-Z1b\_1 and VU108-Z1b\_2) gave plateau ages of 2.67-2.70 Ma which are much higher values than the  
438 biotite inverse isochron ages (2.28-2.31 Ma). This result could be caused by the high <sup>40</sup>Ar/<sup>36</sup>Ar isochron intercepts (>320) with  
439 large uncertainties of ~29. Therefore, on the basis of the remarkable similarity of the two experiments, the combined inverse  
440 isochron age of 2.31 ± 0.28 Ma (MSWD 0.93, <sup>39</sup>Ar<sub>K</sub> 71.36%, <sup>40</sup>Ar\* 34.97%) is considered as the best estimate from amphibole  
441 which overlaps with the biotite age of 2.42 ± 0.03 Ma. This biotite age of 2.42 ± 0.03 Ma is considered to the best approximation  
442 of the eruption age.





443

444

445

446

447

448

**Figure 10.** SiO<sub>2</sub> versus K<sub>2</sub>O (A) and AFM (B) diagrams for the Milos volcanic field with data of this study as solid circles. Published data are represented by shaded fields (Francalanci and Zelmer, 2019 and reference therein). Fields for the tholeiite, calc-alkaline, high-K calc-alkaline and shoshonitic series are from Peccerillo and Taylor (1976). Vertical lines defining fields for basalt, basaltic-andesite, andesite, dacite and rhyolite are from Le Bas et al. (1986). The solid line dividing tholeiitic and calc-alkaline fields is from Irvine and Baragar (1971).

449

### 3.2 Major element results

450

451

452

453

454

455

456

457

458

459

Major-element results are given in Table 4. The major element compositions range from 54 to 78 wt.% SiO<sub>2</sub> (basaltic-andesite-rhyolite to dacite-rhyolite, see Figure 10A). The most felsic samples (SiO<sub>2</sub>>75 wt.%) belong to the Fyriplaka and Trachilas complexes. Our data overlap with those of previous studies and display a similar range in SiO<sub>2</sub>-K<sub>2</sub>O (Francalanci and Zellmer, 2019 and reference therein). The samples of Polyegos are similar to the Fyriplaka and Trachilas complexes, whereas the older Milos samples overlap with Kimolos and Antimilos (Fytikas et al., 1986, Francalanci et al., 2007). Although some samples of Antimilos are tholeiitic, all of the Milos volcanic units belong to the calc-alkaline and medium to high-K series (Figure 10B). A mafic inclusion, sample G15M0022, has high K<sub>2</sub>O (6%), similar to sample G15M0021 (7.2 wt.%). Both of them were collected from the Vani Cape area (Fig. 2). The SiO<sub>2</sub> wt.% versus our <sup>40</sup>Ar/<sup>39</sup>Ar ages diagram (Figure 11A) shows that there is a tendency of the volcanic units to become more felsic over time. In the diagram with K<sub>2</sub>O/SiO<sub>2</sub> versus age there is no significant change (Figure 11C).

460

**Table 4. Major-element composition of volcanic samples from the Milos Volcanic Field.**

Sample-ID	G15M0008	G15M0012	G15M0009	G15M0007	G15M0033	G15M0034	G15M0035	G15M0013	G15M0020	G15M0019	G15M0032B	G15M0004
Rock Types	Pumice	Pumice	Pumice	Pumice	Pumice	Pumice	Pumice	Rhyolite	-	Dacite	Obsidian	Dacite
Period	III								II			
Major elements (wt.%)												
SiO <sub>2</sub>	76.71	75.47	76.02	76.68	76.68	76.89	78.40	72.87	-	64.26	75.57	63.56
TiO <sub>2</sub>	0.14	0.13	0.13	0.08	0.10	0.08	0.08	0.22	-	0.56	0.20	0.57
Al <sub>2</sub> O <sub>3</sub>	12.96	12.77	12.91	12.60	12.86	12.64	12.93	14.11	-	16.08	13.32	16.09
Fe <sub>2</sub> O <sub>3</sub>	1.11	1.08	1.04	0.85	0.88	0.84	0.85	1.95	-	5.33	1.46	5.70

MnO	0.06	0.06	0.06	0.08	0.09	0.09	0.09	0.07	-	0.11	0.06	0.11
MgO	0.22	0.22	0.23	0.11	0.18	0.11	0.11	0.51	-	2.42	0.33	2.81
CaO	1.27	1.27	1.19	0.75	0.85	0.74	0.76	2.23	-	5.33	1.71	6.01
Na <sub>2</sub> O	4.04	4.12	3.99	3.58	3.71	3.50	3.49	3.73	-	3.60	3.95	3.49
K <sub>2</sub> O	3.22	3.15	3.41	4.74	4.46	4.85	4.95	3.43	-	1.69	3.26	1.57
P <sub>2</sub> O <sub>5</sub>	0.02	0.02	0.02	0.01	0.01	0.01	0.01	0.04	-	0.04	0.03	0.09
BaO	0.06	0.06	0.06	0.05	0.05	0.05	0.05	0.06	-	0.04	0.06	0.04
L.O.I.	0.16	0.35	0.16	0.17	0.14	0.33	0.06	0.13	-	0.09	0.07	0.04
Total	99.97	98.70	99.22	99.70	100.01	100.13	101.78	99.35	-	99.55	100.02	100.08

461

Sample-ID	G15M0 021	G15M0 022	G15M0 023	G15M0 024	G15M0 025	G15M0 026	G15M0 006	G15M0 016	G15M0 029	G15M0 015	G15M0 017
Rock Types	Trachy- dacite	Enclave	Dacite	Rhyolite	Dacite	Dacite	Dacite	Basaltic Andesite	Dacite	Dacite	Dacite
Period	II				I						
Major elements (wt.%)											
SiO <sub>2</sub>	64.98	53.87	73.05	76.57	69.56	69.57	68.58	<b>55.72</b>	61.91	63.77	68.03
TiO <sub>2</sub>	0.35	0.60	0.29	0.23	0.42	0.43	0.40	0.66	0.79	0.64	0.58
Al <sub>2</sub> O <sub>3</sub>	16.82	19.91	14.24	11.73	15.30	16.08	15.90	18.43	17.09	16.33	15.90
Fe <sub>2</sub> O <sub>3</sub>	3.69	7.61	3.23	1.69	3.15	3.38	2.67	7.70	5.90	5.42	3.47
MnO	0.08	0.16	0.02	0.03	0.11	0.04	0.07	0.14	0.09	0.10	0.07
MgO	1.50	3.93	0.53	0.46	0.88	0.62	0.81	4.42	1.84	2.48	1.34
CaO	2.19	5.45	2.35	2.36	3.67	3.43	2.89	8.78	6.07	5.91	4.31
Na <sub>2</sub> O	2.61	1.73	3.28	2.85	3.49	3.56	4.19	2.90	3.57	3.35	3.76
K <sub>2</sub> O	7.24	6.11	3.36	2.31	2.98	2.63	3.61	1.41	2.71	1.91	2.69
P <sub>2</sub> O <sub>5</sub>	0.05	0.08	0.04	0.05	0.11	0.09	0.11	0.09	0.20	0.09	0.10
BaO	0.35	0.34	0.06	0.05	0.06	0.06	0.10	0.03	0.13	0.04	0.04
L.O.I.	0.17	0.21	0.12	0.20	0.19	0.09	0.12	0.06	0.09	0.04	0.48
Total	100.03	100.00	100.57	98.53	99.92	99.98	99.45	100.34	100.39	100.08	100.77

462

463

The classification of rock type for each sample is on the basis of field observation and SiO<sub>2</sub> versus K<sub>2</sub>O plot of Le Bas et al. (1986). All iron expressed as Fe<sub>2</sub>O<sub>3</sub>T(otal).

464

### 3.3 Variations of eruption volume with ages

465

466

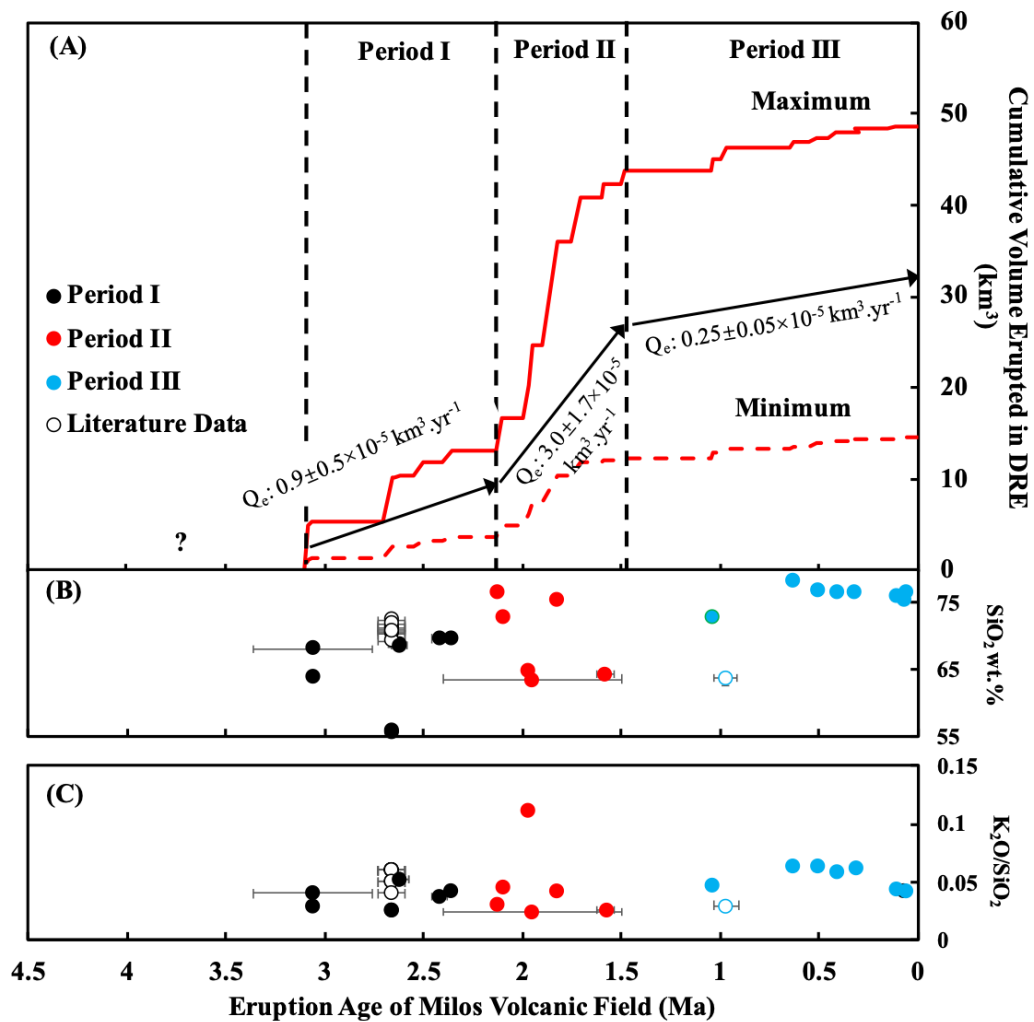
467

468

469

470

Figure 11a shows the cumulative volcanic output volume of the Milos VF over time. This diagram shows that the Milos VF can be separated into three periods: Periods I (~3.3-2.13 Ma) and III (1.48-0.00 Ma) are characterised by low volcanic output volumes, whereas Period II (2.13-1.48 Ma) shows a rapid increase in volcanic output volume. Period I and II are build up in submarine settings, whereas Period III is in a subaerial setting. The Milos VF was largely (~85% by volume) constructed in submarine before ~1.48 Ma (Period I and II) (Figure 11A). During Period III (1.48 Ma-present), only a small volume (~15%) of rhyolitic magma was added from different eruption vents. See the details of Period I-III in section 4.3.2.



471  
472  
473  
474  
475  
476  
477  
478

Figure 11. Eruption age versus (A) cumulative eruption volume for the volcanic deposits of Milos, (B) SiO<sub>2</sub> wt.%, (C) K<sub>2</sub>O%/SiO<sub>2</sub>%, of Milos volcanic units of this study and previous studies. The maximum (Max; red line) and minimum (Min; dashed red line) cumulative eruption volume curves were estimated from Campos et al. (1996) and Stewart and McPhie (2006).  $Q_e$  is the long-term volumetric volcanic output rate (see discussion). The exact volume of volcanic products between 4.1 and 3.08 Ma is not well constrained and indicated with a question mark. The major element data of the old pumices of Filakopi volcanoes (2.66 Ma) are from Stewart (2003). The major element data of the Plakes lava dome is from Fytikas et al. (1986). Geochemical data of the old pumices of the Profitis Ilias (~3.08 Ma) is lacking due to the severe alteration.

#### 479 4 Discussion

480 In this section, our <sup>40</sup>Ar/<sup>39</sup>Ar results are compared with previously published geochronological data, and subsequently used to  
481 refine the stratigraphy of the Milos VF. In the last part, we will discuss the temporal variations in major elements and the  
482 volumetric volcanic output rate of the Milos VF.

#### 483 4.1 Comparison with the previous geochronological studies on the Milos VF

~~484 K-Ar ages may show undesirable and unresolvable scatter due to various problems: (1) inaccurate determination of radiogenic  
485 argon due to either incorporation of excess argon or incomplete degassing of argon during the experiments; (2) inclusion of  
486 cumulate or wall rock phenocrysts in bulk analyses; (3) disturbance of a variety of geological processes such as slow cooling,  
487 thermal reheating; (4) unrecognized heterogeneities due to separate measurements of potassium and argon content by different  
488 methods; (5) requirement of relatively large quantities (milligrams) of pure sample (e.g. Lee, 2015). In addition to these  
489 methodological issues, in the case of Milos we observe that hydrothermal alteration caused substantial kaolinization, in  
490 particular the felsic volcanic samples, that most likely has affected the K-Ar systematics. Some of these issues are also valid  
491 for the <sup>40</sup>Ar/<sup>39</sup>Ar method. However, the K-Ar method does not allow testing if ages are compromised.~~

492 ~~<sup>40</sup>Ar/<sup>39</sup>Ar ages only need isotopes of argon to be measured from a single aliquot of sample with the same equipment that can~~  
493 ~~eliminate some of the problems with sample inhomogeneity. Furthermore, step heating and multiple single fusion experiments~~  
494 ~~can shed light on sample inhomogeneity due to partial alteration effects. The high sensitivity of modern noble gas mass~~  
495 ~~spectrometers for <sup>40</sup>Ar/<sup>39</sup>Ar measurements results in very small sample amounts needed for analysis, that can yield more~~  
496 ~~information on the thermal or alteration histories than larger samples. Moreover, other argon isotopes (<sup>36</sup>Ar, <sup>37</sup>Ar and <sup>38</sup>Ar) can~~  
497 ~~be used to infer some information about the chemical compositions (i.e. Ca and Cl) of samples. A high-resolution laser~~  
498 ~~incremental heating method of <sup>40</sup>Ar/<sup>39</sup>Ar dating allows us to resolve the admixture of phenocryst-hosted inherited <sup>40</sup>Ar in the~~  
499 ~~final temperature steps of the incremental step heating experiments.~~ More than half of our <sup>40</sup>Ar/<sup>39</sup>Ar ages derived for this study  
500 are based on ~~this method~~ high-resolution laser incremental heating method. All incremental step heating experiments are  
501 reproducible, except for the sample G15M0017 which gave the oldest age. The total fusion experiments of this study gave at  
502 least five times smaller analytical uncertainty (1SE on average  $\leq 0.01$  Ma) than the previous studies using conventional K-Ar  
503 (Angelier et al., 1977; Fytikas et al., 1976, 1986; Matsuda et al., 1999) and SHRIMP U/Pb zircon methods (Stewart and  
504 McPhie, 2006). Fission track dating on obsidians of the Milos VF produced two ages (Bigazzi and Radi, 1981; Arias et al.,  
505 2006) which seems to overlap with the K-Ar and <sup>40</sup>Ar/<sup>39</sup>Ar ages, but with larger uncertainty. U/Pb zircon ages could indicate  
506 the timing of zircon formation at high temperature ( $>1000$  °C) in magma chambers significantly prior to volcanic eruption  
507 (e.g. Flowers et al., 2005). On the other hand, the lower closure temperature of K-rich minerals ( $<700$  °C) makes the K-Ar and  
508 <sup>40</sup>Ar/<sup>39</sup>Ar ages better suited to determine the timing of extrusion of volcanic products (e.g. Grove and Harrison, 1996; Cassata  
509 and Renne, 2013).

510 The MSWD value, as a measure of the scatter of the individual step ages, is based on the error enveloping around the data  
511 point. The decrease in error will automatically cause an increase in MSWD (e.g. York, 1968; Wendt and Carl, 1991). The  
512 MSWD values reported in this study are relatively high. In part this is caused by the fact that modern multi-collector mass  
513 spectrometers used for <sup>40</sup>Ar/<sup>39</sup>Ar dating can measure the isotope ratios very precisely, which in turn would increase the MSWD.  
514 It will be more valuable and challenging to find a plateau or isochron age which meets the MSWD criteria ( $<2.5$ ) by modern  
515 multi-collector <sup>40</sup>Ar/<sup>39</sup>Ar dating than by K-Ar or <sup>40</sup>Ar/<sup>39</sup>Ar dating using a single detector instrument (e.g. Mark et al., 2009).  
516 Potential drawbacks of the <sup>40</sup>Ar/<sup>39</sup>Ar method are its dependence on neutron irradiation causing the production of interfering  
517 argon isotopes that need to be corrected for. The uncertainty in the ages of standards that are required to quantify the neutron  
518 flux also needs to be incorporated in the final ages as are uncertainties related to decay constants (supplementary material II).  
519 Finally, recoil can occur during irradiation. Minerals such as biotite can be prone to recoil, yielding slightly older ages (e.g.  
520 Hora et al., 2010).

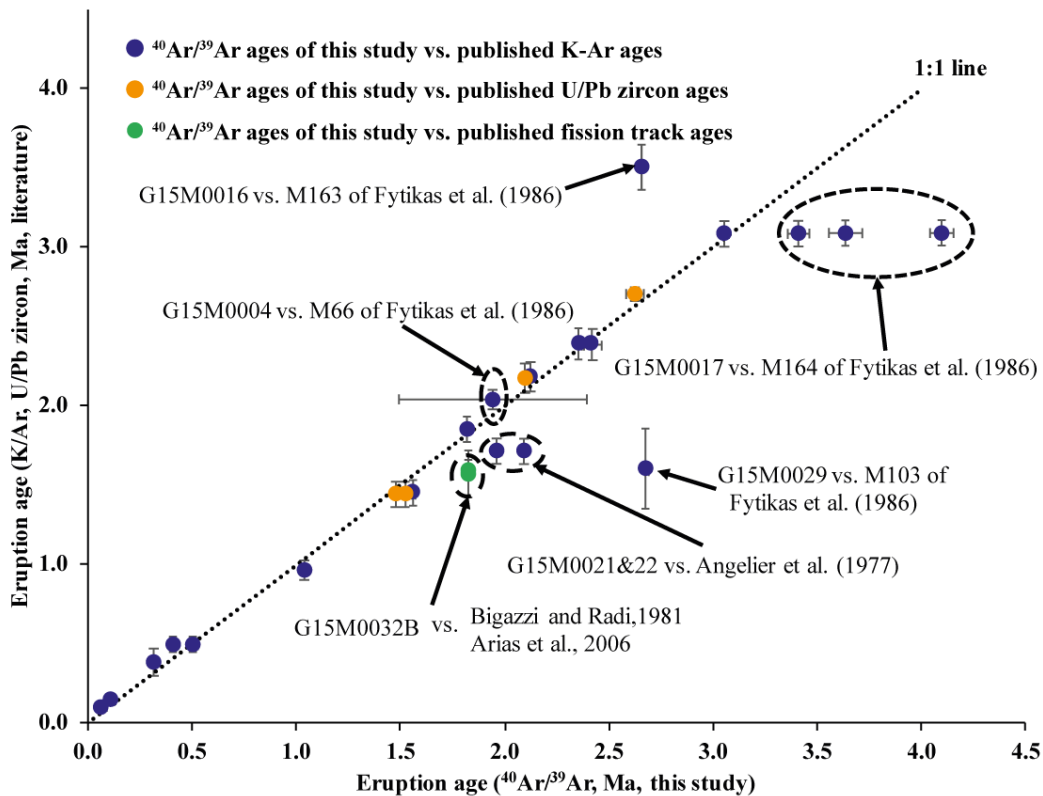
521 Figure 12 compares previous published K-Ar, U/Pb zircon and fission track ages from the same volcanic units with the new  
522 <sup>40</sup>Ar/<sup>39</sup>Ar data of this study. In general, there is a good agreement, however, six ages out of twenty-three differ significantly  
523 from previous studies and will be discussed below.

524 The obsidian fission track ages (Bigazzi and Radi, 1981; Arias et al., 2006) for the Dhemenehaki volcano are 0.25 My younger  
525 than the K-Ar ages (1.84 Ma, Angelier et al., 1977) and the <sup>40</sup>Ar/<sup>39</sup>Ar age of this study (1.825 Ma, G15M0032B). The good  
526 agreement between the K-Ar and <sup>40</sup>Ar/<sup>39</sup>Ar ages suggests that the fission track ages record another, lower temperature event,  
527 than the K-Ar and <sup>40</sup>Ar/<sup>39</sup>Ar ages. In addition, the larger uncertainty of fission track ages ( $>0.05$  Ma) also overlaps with the  
528 <sup>40</sup>Ar/<sup>39</sup>Ar age at 2-sigma. We assume that the <sup>40</sup>Ar/<sup>39</sup>Ar age is the correct extrusion age for the obsidian of the Dhemenehaki  
529 volcano.

530 Angelier et al. (1977) reported one dacite sample in the northwest of Milos with an age of 1.71 Ma (Angelier\_3, location 3 on  
531 Figure 3 of Angelier et al., 1977). Argon loss could result in these ages (Angelier\_3-5 in Figure 12) being younger than our  
532 <sup>40</sup>Ar/<sup>39</sup>Ar groundmass ages of  $1.97 \pm 0.01$  Ma (dacite sample G15M0021 and -22).

533 The amphibole of sample G15M0004 of the Adamas dacitic lava dome, located  $\sim 1$  km north of rhyolitic Bombarda volcano,  
534 gave an inverse isochron age of  $1.95 \text{ Ma} \pm 0.45 \text{ Ma}$ . This age overlaps with the K-Ar age for the Adamas lava dome of  $2.03 \pm$

535 0.06 Ma (dacite M 66) of Fytikas et al. (1986). The large analytical uncertainty of our sample G15M0004 is caused by a  
 536 combination of low  $^{40}\text{Ar}^*$  yields and clustering of data points that define the inverse isochron showing excess argon was  
 537 identified by the  $^{40}\text{Ar}/^{39}\text{Ar}$  method ( $^{40}\text{Ar}/^{36}\text{Ar}$  319.51  $\pm$  14.70), whereas the presence of excess argon cannot be tested by the  
 538 K-Ar technique, implying that the Fytikas et al. (1986) might be slightly old.



539  
 540 **Figure 12. The  $^{40}\text{Ar}/^{39}\text{Ar}$  ages of this study (x-axis) compared to the K/Ar ages (Angelier et al., 1977; Fytikas et al., 1986), U/Pb**  
 541 **zircon ages (Stewart and McPhie, 2006) and fission track ages (Bigazzi and Radi, 1981; Arias et al., 2006) (y-axis) for the same**  
 542 **volcanic units. Ages which deviate from the 1:1 correlation line are discussed in section 4.1.**

543 The Korakia andesite has an age of  $1.59 \pm 0.25$  Ma (M 103, Fytikas et al., 1986) and was deposited in a submarine-subaerial  
 544 environment on top of the Sarakiniko Formation that was dated based on paleomagnetic polarity in combination with a K-Ar  
 545 age (1.80-1.85 Ma, Stewart and McPhie, 2003 and reference therein). The much older  $^{40}\text{Ar}/^{39}\text{Ar}$  groundmass age ( $2.68 \pm 0.01$   
 546 Ma) of Korakia andesite sample G15M0029 is unreliable and it could indicate the emplacement age of the Kalogeros  
 547 cryptodome ( $2.70 \pm 0.04$  Ma, Stewart and McPhie, 2006) or represents a geological meaningless age with only 23-27% of the  
 548 total  $^{39}\text{Ar}$  released in the “plateau”. In this case, the K-Ar age of  $1.59 \pm 0.25$  Ma is considered as the likely eruption age for the  
 549 Korakia andesite although its argon loss or excess Ar component is unknown.

550 We obtained  $^{40}\text{Ar}/^{39}\text{Ar}$  ages of 3.41-4.10 Ma and  $3.06 \pm 0.02$  Ma, respectively, from the groundmasses of dacite samples  
 551 G15M0017 and G15M0015 in the southwest of Milos (Figure 2 and 13B). Both of these samples are derived from the coherent  
 552 dacite facies of the rhyolitic Profitis Illias volcano based on the Figure 11 of Stewart and McPhie (2006). Sample G15M0015  
 553 yielded much higher radiogenic  $^{40}\text{Ar}$  (41.77%) than that of sample G15M0017 (<10% of  $^{40}\text{Ar}^*$ ), and the rhyolite sample M  
 554 164 from Fytikas et al. (1986) (23.5% of  $^{40}\text{Ar}^*$ ) gave an estimate the eruptive age of  $3.08 \pm 0.08$  Ma to the Profitis Illias  
 555 volcano which is much younger than that given by our sample G15M0017 (Figure 12). Therefore, we consider our  $^{40}\text{Ar}/^{39}\text{Ar}$   
 556 ages of  $3.06 \pm 0.02$  Ma as the best estimate of the emplacement age of the coherent dacite facies of Profitis Illias volcano.

557 A basaltic andesite dyke near Kleftiko on the south-western coast of Milos has a K-Ar age of  $3.50 \pm 0.14$  Ma which only gave  
 558 13.9% of  $^{40}\text{Ar}^*$  (Fytikas et al. 1986). This age is significantly older than the eruptive ages of Profitis Illias volcano which the  
 559 dyke intruded (Stewart, 2003). Although containing relatively low  $^{40}\text{Ar}^*$  (16.87%), our  $^{40}\text{Ar}/^{39}\text{Ar}$  age of  $2.66 \pm 0.01$  Ma with  
 560 67.27% of  $^{40}\text{Ar}^*$  from the groundmass of basaltic andesitic sample G15M0016 of the dyke near Kleftiko is probably an accurate  
 561 intrusion age.

## 562 4.2 The published ages of other volcanic units

563 Unfortunately, we were not able to date all key volcanic units of the Milos VF. This was due to three reasons: (1) we did not  
564 collect samples from all units; (2) some of the collected samples were not fresh enough after inspection of thin sections; and  
565 (3) some of the  $^{40}\text{Ar}/^{39}\text{Ar}$  data indicate that the K-Ar decay system was disturbed. Therefore, we include published age  
566 information to establish a complete high-resolution geochronology for the Milos VF.

567 The published volcanic units that we include are the Profitis Ilias volcano ( $3.08 \pm 0.08$  Ma with 23.5 (%), Fytikas et al., 1986),  
568 the Mavro Vouni lava dome ( $2.50 \pm 0.09$  Ma with 55.2  $^{40}\text{Ar}^*$  (%), Anglier et al., 1977) in the south-western part of Milos, the  
569 Bombarda volcano ( $1.71 \pm 0.05$  Ma with 24.3  $^{40}\text{Ar}^*$  (%), Fytikas et al., 1986), the Plakes volcano ( $0.97 \pm 0.06$  Ma with 10.2  
570  $^{40}\text{Ar}^*$  (%), Fytikas et al., 1986, and 0.8-1.2 Ma with 5.4-11.9  $^{40}\text{Ar}^*$  (%) Matsuda et al. 1999). Scoria deposits that Stewart and  
571 McPhie (2006) attributed to an andesitic scoria cone between Milos and Kimolos were produced in submarine, and maybe  
572 occasionally above sea level. No age data for this deposit has been published so far. However, the stratigraphic position of this  
573 scoria deposit is between MIL 365 (2.66 Ma, Stewart and McPhie, 2006) and M103 (1.59 Ma, Fytikas et al., 1986), which is  
574 shown in Figure 10 of Stewart and McPhie (2006). Therefore, this scoria cone was likely active in the north-eastern part of the  
575 Milos VF between 2.6 and 1.6 Ma.

576 Fytikas et al. (1986) also analysed a pumice coming from the Sarakiniko deposits east of Adamas ( $1.85 \pm 0.10$  Ma with 13.6  
577  $^{40}\text{Ar}^*$  (%), Fytikas et al., 1986) (Fig. 2). This unit is reworked pyroclastic sediment of the Adamas lava dome (Rinaldi and  
578 Venuti, 2003). Therefore, the K-Ar age from the Sarakiniko unit is not considered as an eruption age in this study. We did not  
579 sample the neighbouring islands of the Milos VF and also did not attempt to date the products of the recent phase of phreatic  
580 activity from which Traineau and Dalabakis (1989) obtained  $^{14}\text{C}$  ages of 200 BC and 200 AD.

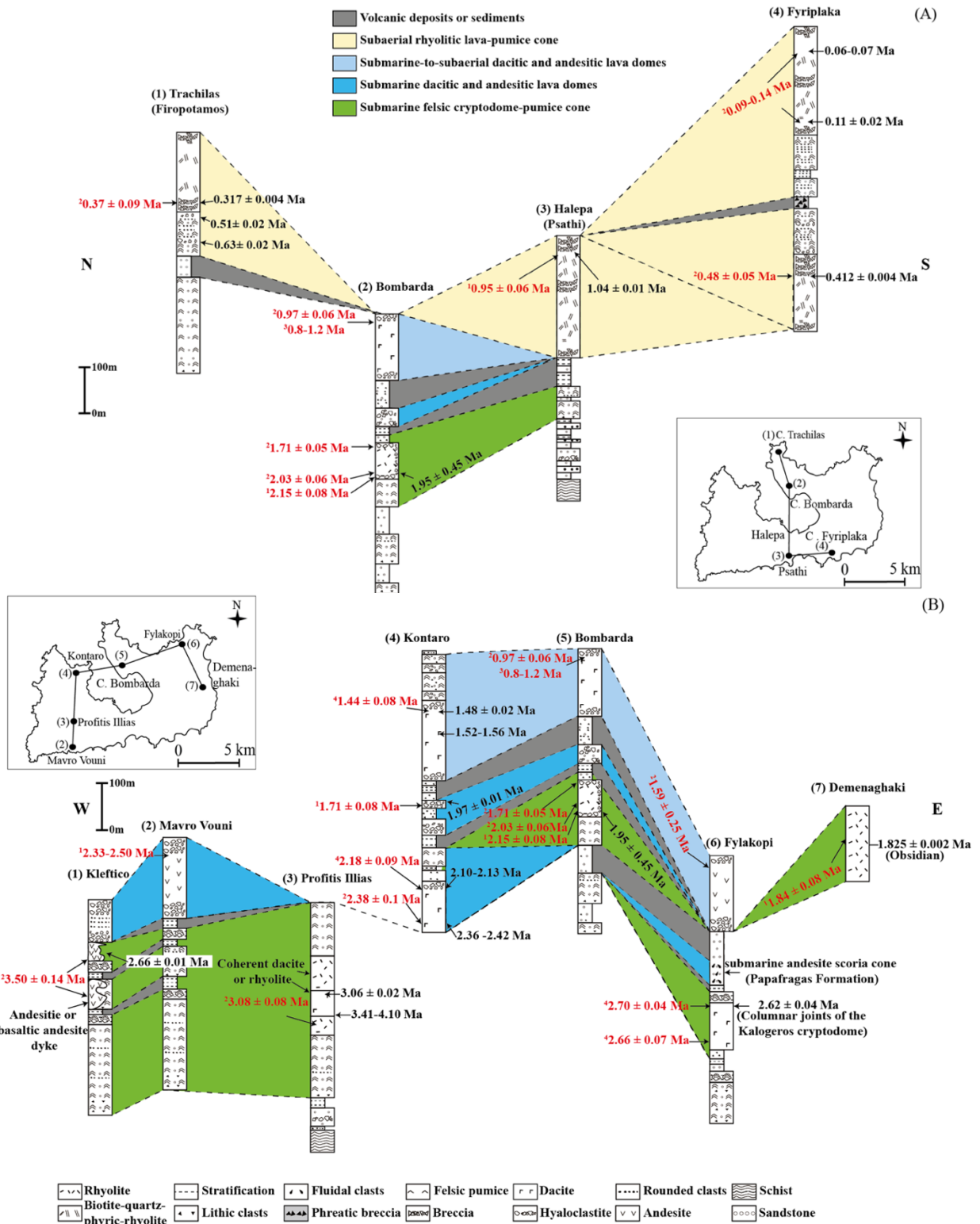
## 581 4.3 Implications for the stratigraphy of the Milos VF

### 582 4.3.1. Start of volcanism in the Milos VF

583 Figures 13 and 14 summarize our new  $^{40}\text{Ar}/^{39}\text{Ar}$  ages in combination with previously published stratigraphic, biostratigraphic,  
584 fission track,  $^{14}\text{C}$ , K-Ar and U-Pb age data. We did not consider the Matsuda et al. (1999) data as the fission-track ages seem  
585 to be offset to other dating techniques ages obtained from the same deposits (see section 4.1 above). The exact start of  
586 volcanism in the Milos VF is still unclear since these older deposits are strongly hydrothermally altered. Van Hinsbergen et al.  
587 (2004) reported five ash layers in the Pliocene sedimentary rocks of southern Milos, ranging between 4.5-3.7 Ma in age, based  
588 on biostratigraphy, magnetostratigraphy and astronomical dating. In a slightly wider circle around Milos island, the  $6.943 \pm$   
589  $0.005$  Ma a1-tephra event recorded in several locations on nearby Crete (Rivera et al., 2011) shows that explosive volcanism  
590 along the Aegean arc, possibly on Milos, already occurred during the Messinian. These ash beds cannot be traced to currently  
591 exposed centres in the Milos VF and could conceivably be related to volcanic centres further north (Antiparos and Patmos),  
592 which were active during this time interval (Vougioukalakis et al., 2019).

593 Biostratigraphy shows that the youngest layer with dateable fossils (bio-event, the last common occurrence of *Sphenolithus*  
594 spp., Van Hinsbergen et al., 2004) in the Neogene sedimentary rocks is 3.61 Ma old (GTS2020, Raffi et al., 2020). The  
595 diatomite Unit II from Calvo et al. (2012) on top of the oldest volcanoclastic deposit from the north-eastern coast of Milos is  
596 constrained within 2.83-3.19 Ma. These data suggest that the oldest products must be older than 2.83 Ma and younger than  
597 3.61 Ma. Our oldest  $^{40}\text{Ar}/^{39}\text{Ar}$  ages of this study displayed a wide range of 3.41-4.10 Ma that is probably not correct due to  
598 alteration of the samples. Alteration might induce Ar loss and that would imply that the age is even older than 3.4-4.1 Ma. The  
599 age of  $3.50 \pm 0.14$  Ma given by Fytikas et al. (1986) for an andesitic pillow lava or dyke has been discussed above and probably  
600 belongs to a series of basaltic andesite intrusions in the younger dacitic-rhyolitic deposits of Profitis Ilias ( $\sim 3.08$  Ma, Fytikas  
601 et al., 1986), and therefore the 3.5 Ma age is probably not correct (e.g. Stewart, 2003). Fytikas et al. (1986) measured one  
602 sample from Kimolos (Figure 2 and 3) with an age of 3.34 Ma. Furthermore, Ferrara et al. (1980) reported an age of 3.15 Ma

603 for a lithic clast derived from the Petalia intrusion in the Kastro volcanoclastics of Polyegos. If we assume that this reported  
 604 age is a cooling age, volcanism in the Milos VF must have started before 3.15 Ma. Although age constraints for the start of  
 605 volcanism on Milos both from the Neogene sedimentary rocks and the dated volcanic samples are poor, the evidence at this  
 606 stage would suggest that volcanism in the Milos VF started ~3.3 Ma ago.



607

608

609 **Figure 13.** Nine selected stratigraphic columns covering the (A) young (<1.4 Ma) and (B) old (>1.4 Ma) volcanic deposits of Milos  
 610 modified after Stewart and McPhie (2006), except for (7) Demenaghaki. Age data in black are from this study and in red are from:  
 611 1=Angelier et al. (1977), 2=Fytikas et al. (1976, 1986), 3=Matsuda et al. (1999), 4=Stewart and McPhie (2006).

612

613 **4.3.2. Periods with different volumetric output**

614 The volume estimates of the Milos VF are hampered by limited exposure of several volcanic units and unknown age  
615 relationships. Therefore, not all units can be attributed to a certain volcano. Furthermore, we also do not know how much the  
616 volcanic products were lost through transport by air, sea currents and erosion. Therefore, the discussion here only provides a  
617 first order estimate of the onshore extruded magma volume. Taken into account all these limitations, our age data and the  
618 volume estimates by Stewart and McPhie (2006) indicate at least three periods of different long-term volumetric volcanic  
619 output rates ( $Q_e$ ) from  $\sim 3.3$  to 0.0 Ma. We define a “Period” as a time interval where the  $Q_e$  is significantly different from the  
620 average output rate ( $Q_e$  average =  $1.0 \times 10^{-5} \text{ km}^3 \cdot \text{yr}^{-1}$ ) of the Milos VF over the last 3.3 Ma. Figure 11 shows that the  $Q_e$  can be  
621 subdivided into two slow-growth periods (I and III) and one period (II) during which the  $Q_e$  was significantly larger.  
622 The lower boundary of Period I is based on our estimate of the oldest volcanic units of Milos at  $\sim 3.3$  Ma. These oldest units  
623 were deposited in the southwest of Milos between  $\sim 3.3$  and 3.08 Ma and include the BPS of Fytikas et al. (1986) and the felsic  
624 pumice cone/crypto dome facies of Stewart and McPhie (2006). These deposits have a minimum thickness of 120 m. The  
625 estimates of the DRE volume and  $Q_e$  of these earliest volcanic deposits are hampered by the lack of precise age information,  
626 the high degree of alteration and structural complexities. Therefore, we only calculated the  $Q_e$  of Period I from 3.08 Ma for  
627 which the eruption products are mainly dacitic-rhyolitic in composition (Table 5, Fig 11), and the first products that can be  
628 reliably dated are cryptodomes (3.06 Ma, sample G15M0015) and dykes (2.66 Ma, sample G15M0016) into the BPS of Fytikas  
629 et al. (1986) or the units of Profitis Illias volcano of Stewart and McPhie (2006, 3.08 Ma) in the southwest of Milos. These  
630 cryptodomes and dykes were followed by the formation of the submarine Fylakopi pumice cone volcano at 2.66 Ma (Stewart  
631 and McPhie, 2006) and Kalogeros cryptodome at 2.62 Ma (sample G15M0006) in the north-eastern part of Milos. These two  
632 pumice cone volcanoes contributed 3-11  $\text{km}^3$  DRE in volume to the Milos VF. The last two volcanic activities of Period I  
633 occurred in the southwest (Mavro Vauni, 2.50 Ma, Angelier et al., 1977) and west of Milos (Mavros Kavos, 2.36 Ma, this  
634 study), respectively, which produced two high-aspect-ratio andesitic-dacitic lava domes with a total volume of 1-3  $\text{km}^3$  DRE  
635 (Stewart and McPhie, 2006). During the submarine Period I, which lasted  $\sim 1.2$  Ma, the estimated  $Q_e$  is  $0.9 \pm 0.5 \times 10^{-5} \text{ km}^3 \cdot \text{yr}^{-1}$ .  
636

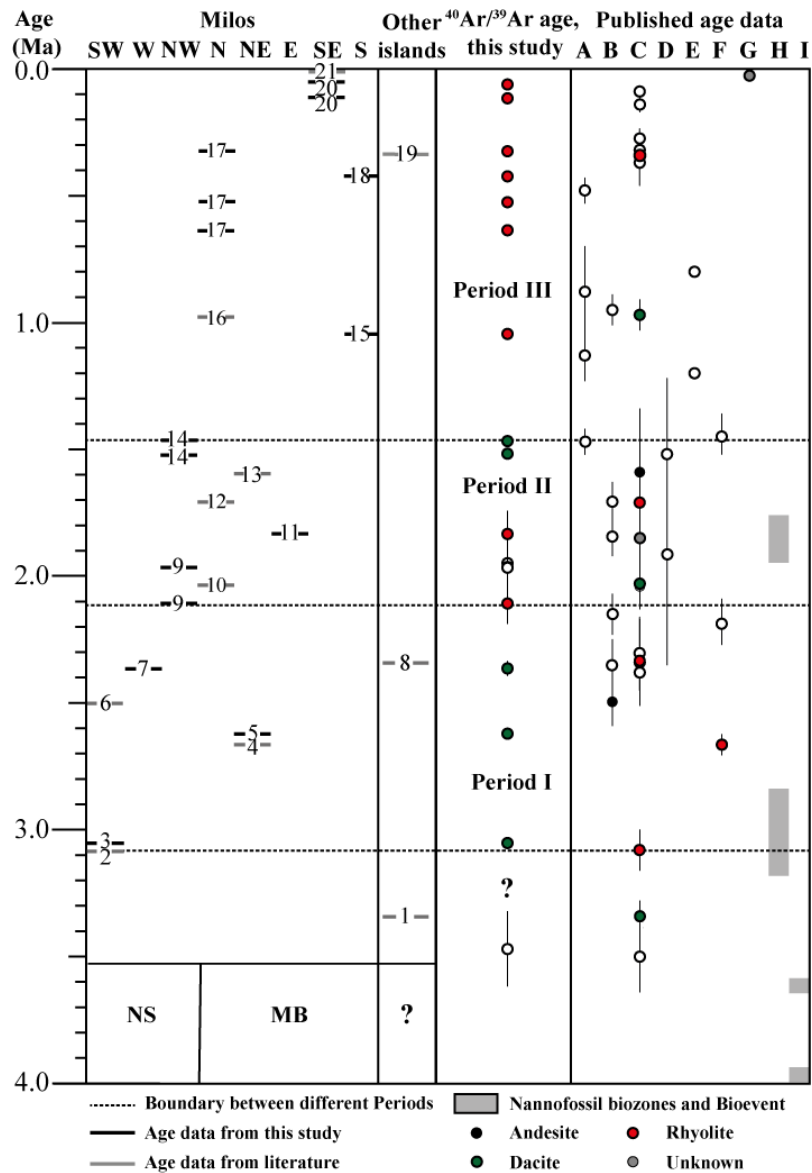
**Table 5. Summary of the eruption ages of the Milos volcanic field**

No.	Name of volcanic centre	Age (Ma)	Reference
1	Kimlos volcano	3.34	Fytikas et al., 1986
2	Profitis Illias crypto/pumice cone	3.08	Fytikas et al., 1986
3	coherent dacite of Profitis Illias volcano	3.06	This study
4	Filakopi volcano	2.66	Stewart and McPhie, 2006
5	Kalegeros cryptodome	2.62	This study
6	Mavro Vouni lava dome	2.5	Angelier et al., 1977
7	Mavros Kavos lava dome	2.42-2.36	This study
8	Polyegos lava dome	2.34	Fytikas et al., 1986
9	Triades lava dome	2.13-2.10 and 1.97	This study
10	Adamas lava dome	2.03	Fytikas et al., 1986
11	Dhemeneghaki volcano	1.83	This study
12	Bombardo volcano	1.71	Fytikas et al., 1986
13	Korakia dome	1.59	Fytikas et al., 1986
14	Komntaro dome	1.52-1.48	This study
15	Halepa lava dome	1.04	This study
16	Plakes lava dome	0.97	Fytikas et al., 1986
17	Trachilias complex	0.63, 0.51 and 0.317	This study
18	Kalamos lava dome	0.41	This study
19	Antimilos domes	0.32	Fytikas et al., 1986
20	Fyriplaka complex	0.11 and 0.07-0.06	This study
21	Phreatic activity	200 AD-200 BC	Trainau and Dalabakis, 1989

637  
638 The change from Period I to II is based on the sharp increase in  $Q_e$  at 2.13 Ma (Fig. 11). During this period the  $Q_e$  ( $3.0 \pm$   
639  $1.7 \times 10^{-5} \text{ km}^3 \cdot \text{yr}^{-1}$ ) increased by a factor of  $\sim 3$  compared to Period I and III. Period II began with the submarine extrusions of  
640 the dacitic-rhyolitic Triades lava dome in the north-west and dacitic Adamas lava dome in the north-east of Milos and was



641 followed by the rhyolitic Dhemenehaki pumice cone/cryptodome and the Bombardo volcano in the north-east of Milos. For  
642 the Bombarda centre a large age range is reported in the literature (1.71-2.15 Ma, Fig. 13B). We did not successfully date  
643 samples from the Bombarda centre, but Rinaldi and Campos Venuti (2003) reported that an age of 1.71 Ma is the best  
644 approximation based on other stratigraphic information. For the Dhemenehaki centre, we obtained a  $^{40}\text{Ar}/^{39}\text{Ar}$  age of  $1.825$   
645  $\pm 0.002$  Ma from obsidian. The Triades, Adamas, Dhemenehaki and Bombarda centres all developed in submarine settings,  
646 as the intercalated sediments from the northern coast of Milos show (Calvo et al., 2012; Fig. 14). The last two volcanic  
647 expressions in Period II consist of two submarine-to-subaerial lava dome extrusions, Kantaro (1.59 Ma, Fytikas et al., 1987)  
648 and Korakia (1.48 Ma, this study) in the north-west and north-east of Milos, respectively. The products of these two centres  
649 are andesitic-dacitic in composition. All volcanic centres of Period II produced 8-30 km<sup>3</sup> DRE in volume for the Milos VF.  
650 Period III began with a time interval of 0.4 Ma with no eruptions and has a very low  $Q_e$  of  $0.25 \pm 0.05 \times 10^{-5}$  km<sup>3</sup>·yr<sup>-1</sup>. The  
651 boundary between Period II and III can be placed at the last eruption of Period II, at the start of the first eruption in the low  
652 output interval, or halfway in between. The difference between those options is not significant, given the large uncertainties  
653 of the volume estimates (Fig. 12), and therefore we have decided to start Period III directly after the last eruption of the high  
654  $Q_e$  of Period II. The composition of nearly all Period III volcanic products is rhyolitic, an exception is the dacitic Plakes lava  
655 dome (Fig. 12). The Plakes lava dome is probably the last volcano erupting at  $\sim 0.97$  Ma (Fytikas et al., 1987) in a submarine  
656 environment in the north of Milos, whereas the other lava dome in Period III, Halepa, produced rhyolitic lavas in a subaerial  
657 setting in the south (Stewart and McPhie, 2006). The Halepa and Plakes domes contributed 1-3 km<sup>3</sup> DRE in volume to the  
658 Milos VF and were followed by a 0.3 Ma interval with no or limited volcanic eruptions. Two subaerial pumice cone volcanoes  
659 with biotite bearing rhyolites were constructed during the last 0.6 Ma, the Trachilias and Fyriplaka complexes. The Trachilias  
660 complex was active for approximately 300 kyr (0.63-0.32 Ma) in the northern part of Milos. The evolution of this complex  
661 began with phreatic eruptions which became less explosive over time (Fytikas et al., 1986). During the last eruption ( $0.317 \pm$   
662  $0.004$  Ma) of the Trachilias complex rhyolitic pumices filled up the crater area and did breach the northern tuff cone walls. The  
663 Trachilias complex only added a small volume (1-2 km<sup>3</sup> DRE) to the Milos VF. The Kalamos lava dome was also extruded in  
664 the south of Milos (Fig. 2) contemporaneously with the Trachilias complex.  
665 The youngest volcanic activity of Milos (0.11 Ma-present) is characterized by subaerial eruptions of biotite phyric rhyolite  
666 from the Fyriplaka complex in the south of Milos, and was studied in detail by Campos Venuti and Rossi (1996). This complex  
667 is constructed on a paleosol that developed in a phreatic deposit ("Green Lahar", Fytikas et al., 1986) or lies directly on the  
668 metamorphic basement. Campos Venuti and Rossi (1996) indicated that the stratigraphic order is: Fyriplaka and Gheraki tuff  
669 rings, Fyriplaka lava flow, tuff cone of Tsigrado-Provatas. The total estimated volume of volcanic material is 0.18 km<sup>3</sup> DRE.  
670 The boundary between the Fyriplaka and Tsigrado tuff cones is characterized by a marked erosive unconformity. The  
671 composition of these young volcanic products is very constant (Fig. 10-11), as noted by Fytikas et al. (1986) and Campos  
672 Venuti and Rossi (1996). The products from Fyriplaka and Tsigrado cones are covered by a paleosol rich in archaeological  
673 remains and a phreatic deposit consisting largely of greenschist metamorphic fragments. According to Campos Venuti and  
674 Rossi (1996), the Fyriplaka cone was quickly built by phreatic and phreatomagmatic eruptions, as there are no paleosols  
675 observed between the different units. However, our data do suggest a large range in ages between 0.11 and 0.06 Ma. Fytikas  
676 et al. (1986) also reported a range between 0.14 and 0.09 Ma. These ages are inconsistent with the "Green Lahar" age of 27  
677 kyrs (Principe et al., 2002), suggesting that the "Green Lahar" deposit consists of many different phreatic eruption layers that  
678 were formed during a time interval of more than 0.4 Ma, as the Kalamos lava is underlain by a green phreatic eruption breccia  
679 (Campos Venuti and Rossi 1996). We, therefore, conclude that phreatic eruptions occurred for more than 400 kyr,  
680 predominantly in the eastern part of Milos until historical times (200 BC – 200 AD, Traineau and Dalabakis, 1989).



681  
682  
683  
684  
685  
686  
687  
688  
689  
690  
691  
692  
693

Figure 14. Diagram presenting three periods of different long-term volumetric volcanic output rate on Milos volcanic field based on the new  $^{40}\text{Ar}/^{39}\text{Ar}$  data of this study and published data. The location of the different volcanoes is given in Fig 2 and indicated in the left panel (from left to right: SW, W, NW, N, NE, E, SE and S of Milos). The right panel corresponds to published age data: [A]=Fytikas et al., 1976, [B]=Angelier et al., 1977, [C]=Fytikas et al., 1986, [D]= Bigazzi & Radi, 1981, [E]=Matsuda, 1999, [F]=Stewart and McPhie (2006), [G]= Trainau and Dalabakis, 1989, and Biostratigraphic data of the Neogene sediments (NG) is from [H]=Calvo et al. (2012) and [I]=Van Hinsbergen et al. (2004) calibrated to Raffi et al. (2020) (LCO of *Sphenolithus* spp. and FO of *D. tamalis*). The number in the left panel represents the volcanic centres of Milos (see details in Table 5). The start of volcanism (3.08-3.61 Ma) on Milos and the basement of the other Islands (Antimilos, Kimolos and Polyegos) are not well constrained and indicated with question marks (see text for discussion). The simplified basement cross-section (NS: Neogene sedimentary rock; MB: Metamorphic basement) under Milos volcanic units is based on Fytikas et al. (1989). We used the filled symbols as the best estimate for the eruption ages at the different volcanic centres, and the open symbols are not used as the best estimate due to their relatively large uncertainties.

### 694 4.3.3 Temporal evolution of the magma flux and composition

695 Figure 11 shows temporal major-element variations during the evolution of the Milos VF. The volcanic units of Period III are  
696 dominantly rhyolitic in composition, whereas during Period I and II the compositions of volcanic units range between basaltic-  
697 andesite to rhyolite. However, the  $\text{K}_2\text{O}/\text{SiO}_2$  ratio is constant ( $0.05 \pm 0.02$ ) over the 3.3 Ma evolution of the Milos VF, with  
698 one exception, sample G15M0021 collected near Cape Vani which is altered by hydrothermal processes (e.g. Alfieris et al.  
699 2013). Period I and III contain large explosive pumice cone volcanoes, whereas Period II is dominated by effusive dome  
700 extrusions. The difference in volcanic structures is not observed in the  $\text{SiO}_2$  content and the  $\text{K}_2\text{O}/\text{SiO}_2$  ratio of the volcanic  
701 products.

702 It is noteworthy that the value of the  $Q_e$  ( $0.2-4.7 \times 10^{-5} \text{ km}^3 \cdot \text{yr}^{-1}$ ) for the Milos VF is at least 2-3 orders lower than the average  
703 for rhyolitic systems ( $4.0 \times 10^{-3} \text{ km}^3 \cdot \text{yr}^{-1}$ ) and the mean for continental arcs ( $\sim 70 \times 10^{-3} \text{ km}^3 \cdot \text{yr}^{-1}$ ) (White et al., 2006). Milos  
704 overlaps with the lowest  $Q_e$  values of the study of White et al. (2006). No data are available for the ratio between intruded  
705 magma in the crust below Milos and extruded volcanic units (I:E). White et al. (2006) argued that a ratio of 5:1 (I:E) is probably  
706 a realistic estimate for most volcanic centres and that this ratio can be higher in volcanic centres constructed on continental  
707 crust. A magma supply rate from the mantle beneath the Milos VF could be estimated in the order of  $0.1-3.3 \times 10^{-4} \text{ km}^3 \cdot \text{yr}^{-1}$ .  
708 Druitt et al. (2019) reported a long-term average magma supply rate of approximately  $1 \times 10^{-3} \text{ km}^3 \cdot \text{yr}^{-1}$  beneath the Kameni  
709 islands of Santorini, which is comparable to that of the Milos. Besides the case of Santorini VF, no other information on the  
710 long-term average magma supply rate of other volcanic centres of the SAVA is available to our knowledge.  
711 Milos is approximately 15 km long (W-E), a magma production rate of approximately  $0.7-22 \text{ km}^3 \cdot \text{km}^{-1} \cdot \text{Ma}^{-1}$  can be estimated  
712 over the last  $\sim 3.34$  Ma. Although this magma production rate per km arc length is the onshore estimate for the Milos VF, it is  
713 still significantly lower than for oceanic arcs:  $157-220 \text{ km}^3 \cdot \text{Ma}^{-1} \cdot \text{km}^{-1}$  (Jicha and Jagoutz, 2015). For continental arcs, the long-  
714 term magma production rate is more difficult to establish because magmatism is cyclic, and short periods (5-20 Ma) of intense  
715 magmatism (“flare ups”) with  $85 \text{ km}^3 \cdot \text{km}^{-1} \cdot \text{Ma}^{-1}$  being alternated with periods of 25-50 Ma of low magma production rate of  
716  $20 \text{ km}^3 \cdot \text{km}^{-1} \cdot \text{Ma}^{-1}$  (e.g. Jicha and Jagoutz, 2015). The periods of low magma production overlap with the magma production  
717 rates beneath the Milos VF over the past  $\sim 3.34$  Ma.

## 718 5 Conclusions

719 This study reports twenty-one new  $^{40}\text{Ar}/^{39}\text{Ar}$  ages and major element data for 10 volcanic units of the Milos Volcanic Field.  
720 In combination with previously published age data, geochemistry and facies analysis the following points can be made.

- 721 (1) The exact age of the start of volcanism in the Milos VF is still unclear due to the high degree of alteration of the oldest  
722 deposits. The best estimate based on our new  $^{40}\text{Ar}/^{39}\text{Ar}$  ages, published K-Ar data and nannofossil biozones is between  
723 3.5 and 3.15 Ma.
- 724 (2) Based on the long-term volumetric volcanic output rate, the volcanic history of the Milos VF can be divided into two  
725 slow growth periods, Period I ( $\sim 3.3-2.13$  Ma) and III (1.48 Ma-present), and one relatively fast growth period, Period  
726 II (2.13-1.48 Ma).
- 727 (3) Period I and II are characterised by andesitic to rhyolitic lavas and pyroclastic units, whereas those of Period III are  
728 dominantly rhyolitic. The  $\text{K}_2\text{O}/\text{SiO}_2$  ratio is constant over the 3.3 Ma history of the Milos VF.
- 729 (4) The long-term volumetric volcanic output rate of Milos is  $0.2-4.7 \times 10^{-5} \text{ km}^3 \cdot \text{yr}^{-1}$ , two-three orders of magnitude lower  
730 than the average for rhyolitic systems and continental arcs.

## 731 Acknowledgement

732 We would like to thank Roel van Elsas for the assistance with rock crushing and mineral separation. Kiki Dings helped with  
733 the XRF bead preparation and measurements. Lara Borst and Onno Postma assisted with the  $^{40}\text{Ar}/^{39}\text{Ar}$  dating. We acknowledge  
734 the Greek Institute of Geology and Mineral Exploration (IGME) for permission to conduct fieldwork on Milos. Xiaolong Zhou  
735 would like to acknowledge a grant no. 201506400055 from the China Scholarship Council (CSC). The  $^{40}\text{Ar}/^{39}\text{Ar}$  facility of the  
736 VU is covered by NWO grant 834.09.004. This research benefitted from funding from the European Research Council under  
737 the European Union's Seventh Framework Programme (FP7/2007-2013)/ERC grant agreement n° 319209. A previous version  
738 of this manuscript greatly benefitted from a very detailed and constructive review by Dr. J. McPhie. A second review by Dr J.  
739 McPhie, Dr. J-F. Wotzlav and Dr. Peter Abbott helped to clarify the interpretation of the geochronology of Milos. We thank  
740 Drs. J. Nadden, J. Miles and S Tapster for pointing out mistakes in our figures.

741 **References**

- 742 Alfieris, D., Voudouris, P. and Spry, P. G.: Shallow submarine epithermal Pb-Zn-Cu-Au-Ag-Te mineralization on western  
743 Milos Island, Aegean Volcanic Arc, Greece: Mineralogical, geological and geochemical constraints, *Ore Geol. Rev.*, 53,  
744 159–180, doi:10.1016/j.oregeorev.2013.01.007, 2013.
- 745 Angelier, J., Cantagrel, J.-M. and Vilminot, J.-C.: Neotectonique cassante et volcanisme plio-quadernaire dans l'arc egeen  
746 interne; l'île de Milos (Grece), *Bull. la Société Géologique Fr.*, 7(1), 119–124, 1977.
- 747 Arias, A., Oddone, M., Bigazzi, G., Di Muro, A., Principe, C. and Norelli, P.: New data for the characterization of Milos  
748 obsidians, *J. Radioanal. Nucl. Chem.*, 268(2), 371–386, doi:10.1007/s10967-006-0183-9, 2006.
- 749 Berger, G. W. and York, D.: Geothermometry from  $^{40}\text{Ar}/^{39}\text{Ar}$  dating experiments, *Geochim. Cosmochim. Acta*, 45(6), 795–  
750 811, doi:10.1016/0016-7037(81)90109-5, 1981.
- 751 Bigazzi, G. and Radi, G.: Datazione con le tracce di fissione per l'identificazione della provenienza dei manufatti di  
752 ossidiana, *Riv. di Sci. Preist.*, 36/1–2, 223–250, 1981.
- 753 Calvo, J. P., Triantaphyllou, M. V., Regueiro, M. and Stamatakis, M. G.: Alternating diatomaceous and volcanoclastic  
754 deposits in Milos Island, Greece. A contribution to the upper Pliocene-lower Pleistocene stratigraphy of the Aegean Sea,  
755 *Palaeogeogr. Palaeoclimatol. Palaeoecol.*, 321–322, 24–40, doi:10.1016/j.palaeo.2012.01.013, 2012.
- 756 Campos Venuti, M. and Rossi, P. L.: Depositional facies in the Fyriplaka rhyolitic tuff ring, Milos Island (Cyclades, Greece),  
757 *Acta Vulcanol.*, 8, 173–192, 1996.
- 758 Cassata, W. S. and Renne, P. R.: Systematic variations of argon diffusion in feldspars and implications for  
759 thermochronometry, *Geochim. Cosmochim. Acta*, 112, 251–287, doi:10.1016/j.gca.2013.02.030, 2013.
- 760 Cole, P. D., Calder, E. S., Sparks, R. S. J., Clarke, A. B., Druitt, T. H., Young, S. R., Herd, R. A., Harford, C. L. and Norton,  
761 G. E.: Deposits from dome-collapse and fountain-collapse pyroclastic flows at Soufrière Hills Volcano, Montserrat, *Geol.*  
762 *Soc. London, Mem.*, 21(1), 231–262, 2002.
- 763 Crossweller, H. S., Arora, B., Brown, S. K., Cottrell, E., Deligne, N. I., Guerrero, N. O., Hobbs, L., Kiyosugi, K., Loughlin,  
764 S. C. and Lowndes, J.: Global database on large magnitude explosive volcanic eruptions (LaMEVE), *J. Appl. Volcanol.*,  
765 1(1), 4, 2012.
- 766 Druitt, T. H., Edwards, L., Mellors, R. M., Pyle, D. M., Sparks, R. S. J., Lanphere, M., Davies, M. and Barreirio, B.:  
767 Santorini Volcano, *Geol. Soc. Mem.*, 19 [online] Available from: <http://pubs.er.usgs.gov/publication/70094778>, 1999.
- 768 Druitt, T. H., Pyle, D. M. and Mather, T. A.: Santorini Volcano and its Plumbing System, *Elements*, 15(3), 177–184,  
769 doi:10.2138/gselements.15.3.177, 2019.
- 770 Duermeijer, C. E., Nyst, M., Meijer, P. T., Langereis, C. G. and Spakman, W.: Neogene evolution of the Aegean arc:  
771 Paleomagnetic and geodetic evidence for a rapid and young rotation phase, *Earth Planet. Sci. Lett.*, 176(3–4), 509–525,  
772 doi:10.1016/S0012-821X(00)00023-6, 2000.
- 773 Ferrara, G., Fytikas, M., Giuliani, O. and Marinelli, G.: Age of the formation of the Aegean active volcanic arc, *Thera*  
774 *Aegean world II*, 2, 37–41, 1980.
- 775 Flowers, R. M., Bowring, S. A., Tulloch, A. J. and Klepeis, K. A.: Tempo of burial and exhumation within the deep roots of  
776 a magmatic arc, Fiordland, New Zealand, *Geology*, 33(1), 17–20, doi:10.1130/G21010.1, 2005.
- 777 Francalanci, L. and Zellmer, G. F.: Magma Genesis at the South Aegean Volcanic Arc, *Elements*, 15(3), 165–170,  
778 doi:10.2138/gselements.15.3.165, 2019.
- 779 Francalanci, L., Vougioukalakis, G. E., Fytikas, M., Beccaluva, L., Bianchini, G. and Wilson, M.: Petrology and  
780 volcanology of Kimolos and Polyegos volcanoes within the context of the South Aegean arc, Greece, *Spec. Pap. Soc. Am.*,  
781 418, 33, 2007.
- 782 Frey, H. M., Lange, R. A., Hall, C. M. and Delgado-Granados, H.: Magma eruption rates constrained by  $^{40}\text{Ar}/^{39}\text{Ar}$   
783 chronology and GIS for the Ceboruco-San Pedro volcanic field, western Mexico, *Bull. Geol. Soc. Am.*, 116(3–4), 259–276,

784 doi:10.1130/B25321.1, 2004.

785 Fytikas, M., Giuliani, O., Innocenti, F., Marinelli, G. and Mazzuoli, R.: Geochronological data on recent magmatism of the  
786 Aegean Sea, *Tectonophysics*, 31(1–2), T29–T34, doi:10.1016/0040-1951(76)90161-X, 1976.

787 Fytikas, M., 1977. *Geology and Geothermics of Milos Island*. Thesis, Thessaloniki University, 228 pp. (in Greek with  
788 English summary).

789 Fytikas, M., Innocenti, F., Kolios, N., Manetti, P., Mazzuoli, R., Poli, G., Rita, F. and Villari, L.: Volcanology and petrology  
790 of volcanic products from the island of Milos and neighbouring islets, *J. Volcanol. Geotherm. Res.*, 28(3–4), 297–317,  
791 doi:10.1016/0377-0273(86)90028-4, 1986.

792 Fytikas, M.: Updating of the geological and geothermal research on Milos island, *Geothermics*, 18(4), 485–496,  
793 doi:10.1016/0375-6505(89)90051-5, 1989.

794 Grasemann, B., Huet, B., Schneider, D. A., Rice, A. H. N., Lemonnier, N. and Tschegg, C.: Miocene postorogenic extension  
795 of the Eocene synorogenic imbricated Hellenic subduction channel: New constraints from Milos (Cyclades, Greece), *Bull.*  
796 *Geol. Soc. Am.*, 130(1–2), 238–262, doi:10.1130/B31731.1, 2018.

797 Grove, M. and Harrison, T. M.:  $^{40}\text{Ar}^*$  diffusion in Fe-rich biotite, *Am. Mineral.*, 81(7–8), 940–951, 1996.

798 Hayes, G. P., Moore, G. L., Portner, D. E., Hearne, M., Flamme, H., Furtney, M. and Smoczyk, G. M.: Slab2, a  
799 comprehensive subduction zone geometry model, *Science* (80- ), 362(6410), 58–61, doi:10.1126/science.aat4723, 2018.

800 Hildreth, W. and Lanphere, M. A.: Potassium-argon geochronology of a basalt-andesite-dacite arc system: The Mount  
801 Adams volcanic field, Cascade Range of southern Washington, *Geol. Soc. Am. Bull.*, 106(11), 1413–1429, 1994.

802 Hildreth, W., Fierstein, J. and Lanphere, M.: Eruptive history and geochronology of the Mount Baker volcanic field,  
803 Washington, *Geol. Soc. Am. Bull.*, 115(6), 729–764, 2003a.

804 Hildreth, W., Lanphere, M. A. and Fierstein, J.: Geochronology and eruptive history of the Katmai volcanic cluster, Alaska  
805 Peninsula, *Earth Planet. Sci. Lett.*, 214(1–2), 93–114, doi:10.1016/S0012-821X(03)00321-2, 2003b.

806 Van Hinsbergen, D. J. J., Snel, E., Garstman, S. A., Marunțeanu, M., Langereis, C. G., Wortel, M. J. R. and Meulenkamp, J.  
807 E.: Vertical motions in the Aegean volcanic arc: Evidence for rapid subsidence preceding volcanic activity on Milos and  
808 Aegina, *Mar. Geol.*, 209(1–4), 329–345, doi:10.1016/j.margeo.2004.06.006, 2004.

809 Hora, J. M., Singer, B. S., Jicha, B. R., Beard, B. L., Johnson, C. M., de Silva, S. and Salisbury, M.: Volcanic biotite-  
810 sanidine  $^{40}\text{Ar}/^{39}\text{Ar}$  age discordances reflect Ar partitioning and pre-eruption closure in biotite, *Geology*, 38(10), 923–926,  
811 doi:10.1130/G31064.1, 2010.

812 IJlst, L.: A laboratory overflow-centrifuge for heavy liquid mineral separation, *Am. Mineral.*, 58, 1088–1093, 1973.

813 Jicha, B. R. and Jagoutz, O.: Magma production rates for intraoceanic arcs, *Elements*, 11(2), 105–112,  
814 doi:10.2113/gselements.11.2.105, 2015.

815 Kiliass, S. P., Naden, J., Cheliotis, I., Shepherd, T. J., Constandinidou, H., Crossing, J. and Simos, I.: Epithermal gold  
816 mineralisation in the active Aegen volcanic arc: The Profitis Ilias deposits, Milos Island, Greece, *Miner. Depos.*, 36(1), 32–  
817 44, doi:10.1007/s001260050284, 2001.

818 Koppers, A. A. P.: ArArCALC-software for  $^{40}\text{Ar}/^{39}\text{Ar}$  age calculations, *Comput. Geosci.*, 28(5), 605–619,  
819 doi:10.1016/S0098-3004(01)00095-4, 2002.

820 Kornprobst, J., Kienast, J.-R. and Vilminot, J.-C.: The high-pressure assemblages at Milos, Greece, *Contrib. to Mineral.*  
821 *Petrol.*, 69(1), 49–63, doi:10.1007/bf00375193, 1979.

822 Kuiper, K. F., Deino, A., Hilgen, F. J., Krijgsman, W., Renne, P. R. and Wijbrans, J. R.: Synchronizing Rock Clocks of  
823 Earth History, *Science* (80- ), 320(5875), 500–504, doi:10.1126/science.1154339, 2008.

824 Lee, J. K. W.: Ar–Ar and K–Ar Dating BT - *Encyclopedia of Scientific Dating Methods*, edited by W. Jack Rink and J. W.  
825 Thompson, pp. 58–73, Springer Netherlands, Dordrecht., 2015.

826 Lee, J. Y., Marti, K., Severinghaus, J. P., Kawamura, K., Yoo, H. S., Lee, J. B. and Kim, J. S.: A redetermination of the

827 isotopic abundances of atmospheric Ar, *Geochim. Cosmochim. Acta*, 70(17), 4507–4512, doi:10.1016/j.gca.2006.06.1563,  
828 2006.

829 Mark, D. F., Barfod, D., Stuart, F. M. and Imlach, J.: The ARGUS multicollector noble gas mass spectrometer: Performance  
830 for  $^{40}\text{Ar}/^{39}\text{Ar}$  geochronology, *Geochemistry, Geophys. Geosystems*, 10(10), 1–9, doi:10.1029/2009GC002643, 2009.

831 Matsuda, J., Senoh, K., Maruoka, T., Sato, H. and Mitropoulos, P.: K-Ar ages of the Aegean the volcanic rocks and arc-  
832 trench system their implication for the arc-trench system, *Geochem. J.*, 33, 369–377, 1999.

833 McKenzie, D.: Active tectonics of the Alpine—Himalayan belt: the Aegean Sea and surrounding regions, *Geophys. J. Int.*,  
834 55(1), 217–254, 1978.

835 Meulenkamp, J. E., Wortel, M. J. R., van Wamel, W. A., Spakman, W. and Hoogerduyn Strating, E.: On the Hellenic  
836 subduction zone and the geodynamic evolution of Crete since the late Middle Miocene, *Tectonophysics*, 146(1–4), 203–215,  
837 doi:10.1016/0040-1951(88)90091-1, 1988.

838 Min, K., Mundil, R., Renne, P. R. and Ludwig, K. R.: A test for systematic errors in  $^{40}\text{Ar}/^{39}\text{Ar}$  geochronology, *Geochim.*  
839 *Cosmochim. Acta*, 64(1), 73–98, 2000.

840 Nicholls, I. A.: Santorini volcano, greece - tectonic and petrochemical relationships with volcanics of the Aegean region,  
841 *Tectonophysics*, 11(5), 377–385, doi:10.1016/0040-1951(71)90026-6, 1971.

842 Pe-Piper, G. and Piper, D. J. W.: The South Aegean active volcanic arc: relationships between magmatism and tectonics,  
843 *Dev. Volcanol.*, 7(C), 113–133, doi:10.1016/S1871-644X(05)80034-8, 2005.

844 Pe-Piper, G. and Piper, D. J. W.: Neogene backarc volcanism of the Aegean: New insights into the relationship between  
845 magmatism and tectonics, *Geol. Soc. Am. Spec. Pap.*, 418(02), 17–31, doi:10.1130/2007.2418(02), 2007.

846 Pe-Piper, G. and Piper, D. J. W.: The effect of changing regional tectonics on an arc volcano: Methana, Greece, *J. Volcanol.*  
847 *Geotherm. Res.*, 260, 146–163, doi:10.1016/j.jvolgeores.2013.05.011, 2013.

848 Principe C, Arias A, Zoppi U.: Origin, transport and deposition of a debris avalanche de- posit of phreatic origin on Milos  
849 Island (Greece). Montagne Pelee 1902-2002, Explosive Vol- canism in Subduction Zones, Martinique 12-16 May,  
850 2002. Abstracts p. 71, 2002.

851 Raffi, I., Wade, B. S., Pälke, H., Beu, A. G., Cooper, R., Crundwell, M. P., Krijgsman, W., Moore, T., Raine, I. and  
852 Sardella, R.: The Neogene Period, in *Geologic Time Scale 2020*, pp. 1141–1215, Elsevier., 2020.

853 Rinaldi, M. and Venuti, M. C.: The submarine eruption of the Bombarda volcano, Milos Island, Cyclades, Greece, *Bull.*  
854 *Volcanol.*, 65(4), 282–293, doi:10.1007/s00445-002-0260-z, 2003.

855 Rivera, T. A., Storey, M., Zeeden, C., Hilgen, F. J. and Kuiper, K.: A refined astronomically calibrated  $^{40}\text{Ar}/^{39}\text{Ar}$  age for  
856 Fish Canyon sanidine, *Earth Planet. Sci. Lett.*, 311(3–4), 420–426, doi:10.1016/j.epsl.2011.09.017, 2011.

857 Rontogianni, S., Konstantinou, N. S., Melis, C. P. and Evangelidis: Slab stress field in the Hellenic subduction zone as  
858 inferred from intermediate-depth earthquakes, *Earth, Planets Sp.*, 63(2), 139–144, doi:10.5047/eps.2010.11.011, 2011.

859 Schaen, A., Jicha, B., Hodges, K., Vermeesch, P., Stelten, M., Mercer, C., Phillips, D., Rivera, T., Jourdan, F., Matchan, E.,  
860 Hemming, S., Morgan, L., Kelley, S., Cassata, W., Heizler, M., Vasconcelos, P., Benowitz, J., Koppers, A., Mark, D.,  
861 Niespolo, E., Sprain, C., Hames, W., Kuiper, K., Turrin, B., Renne, P., Ross, J., Nomade, S., Guillou, H., Webb, L., Cohen,  
862 B., Calvert, A., Joyce, N., Ganerød, M., Wijbrans, J., Ishizuka, O., He, H., Ramirez, A., Pfänder, J., Lopez-Martínez, M.,  
863 Qiu, H. and Singer, B.: Interpreting and reporting  $^{40}\text{Ar}/^{39}\text{Ar}$  geochronologic data, *GSA Bull.*, doi:10.1130/B35560.1, 2020.

864 Singer, B. S., Thompson, R. A., Dungan, M. A., Feeley, T. C., Nelson, S. T., Pickens, J. C., Brown, L. L., Wulff, A. W.,  
865 Davidson, J. P. and Metzger, J.: Volcanism and erosion during the past 930 k.y. at the Tatara–San Pedro complex, Chilean  
866 Andes, *Geol. Soc. Am. Bull.*, 109(2), 127–142, doi:10.1130/0016-7606(1997)109<0127:VAEDTP>2.3.CO;2, 1997.

867 Sonder, R. A.: Zur Geologie and Petrographie der Inselgruppe von Milos, *Zeitschr. Volc.*, 8, 11–231, 1924.

868 Spakman, W., Wortel, M. J. R. and Vlaar, N. J.: The Hellenic Subduction Zone: A tomographic image and its geodynamic  
869 implications, *Geophys. Res. Lett.*, 15(1), 60–63, doi:10.1029/GL015i001p00060, 1988.

870 Stewart, A. L.: Volcanic Facies Architecture and Evolution of Milos, Greece, University of Tasmania., 2003.  
871 Stewart, A. L. and McPhie, J.: Internal structure and emplacement of an Upper Pliocene dacite cryptodome, Milos Island,  
872 Greece, *J. Volcanol. Geotherm. Res.*, 124(1–2), 129–148, doi:10.1016/S0377-0273(03)00074-X, 2003.  
873 Stewart, A. L. and McPhie, J.: An Upper Pliocene coarse pumice breccia generated by a shallow submarine explosive  
874 eruption, Milos, Greece, *Bull. Volcanol.*, 66(1), 15–28, doi:10.1007/s00445-003-0292-z, 2004.  
875 Stewart, A. L. and McPhie, J.: Facies architecture and Late Pliocene – Pleistocene evolution of a felsic volcanic island,  
876 Milos, Greece, *Bull. Volcanol.*, 68(7–8), 703–726, doi:10.1007/s00445-005-0045-2, 2006.  
877 Traineau, H. and Dalabakis, P.: Mise en evidence d’une eruption phreatique historique sur l’île de Milos (Grece), *CR Acad*  
878 *Sci Paris*, 1–38, 1989.  
879 Vougioukalakis, G. E., Satow, C. G. and Druitt, T. H.: Volcanism of the South Aegean volcanic arc, *Elements*, 15(3), 159–  
880 164, 2019.  
881 Wendt, I. and Carl, C.: The statistical distribution of the mean squared weighted deviation, *Chem. Geol. Isot. Geosci. Sect.*,  
882 86(4), 275–285, doi:10.1016/0168-9622(91)90010-T, 1991.  
883 White, S. M., Crisp, J. A. and Spera, F. J.: Long-term volumetric eruption rates and magma budgets, *Geochemistry,*  
884 *Geophys. Geosystems*, 7(3), 262–266, doi:10.1029/2005GC001002, 2006.  
885 York, D.: Least squares fitting of a straight line with correlated errors, *Earth Planet. Sci. Lett.*, 5(C), 320–324,  
886 doi:10.1016/s0012-821x(68)80059-7, 1968.  
887